



**HAL**  
open science

## Propagation of a strike-slip plate boundary within an extensional environment: the westward propagation of the North Anatolian Fault

Xavier Le Pichon, A. M. Celal Sengor, Julia Kende, Caner Imren, Pierre Henry, Celine Grall, Hayrullah Karabulut

### ► To cite this version:

Xavier Le Pichon, A. M. Celal Sengor, Julia Kende, Caner Imren, Pierre Henry, et al.. Propagation of a strike-slip plate boundary within an extensional environment: the westward propagation of the North Anatolian Fault. *Canadian journal of earth sciences*, 2016, 53 (11), pp.1416-1439. 10.1139/cjes-2015-0129 . hal-01765494

**HAL Id: hal-01765494**

**<https://hal.science/hal-01765494v1>**

Submitted on 1 Sep 2024

**HAL** is a multi-disciplinary open access archive for the deposit and dissemination of scientific research documents, whether they are published or not. The documents may come from teaching and research institutions in France or abroad, or from public or private research centers.

L'archive ouverte pluridisciplinaire **HAL**, est destinée au dépôt et à la diffusion de documents scientifiques de niveau recherche, publiés ou non, émanant des établissements d'enseignement et de recherche français ou étrangers, des laboratoires publics ou privés.



**Propagation of a strike slip plate boundary within an extensional environment: the westward propagation of the North Anatolian Fault**

Journal:	<i>Canadian Journal of Earth Sciences</i>
Manuscript ID	cjes-2015-0129.R1
Manuscript Type:	Article
Date Submitted by the Author:	15-Oct-2015
Complete List of Authors:	Le Pichon, Xavier; Collège de France Şengör, Celâl; İstanbul Teknik Üniversitesi, Maden Fakültesi Jeoloji Bölümü Ayazağa Kende, Julia; CEREGE, CNRS-Aix Marseille Université İmren, Caner; İstanbul Teknik Üniversitesi, Henry, Pierre; CEREGE, CNRS-Aix Marseille Université Grall, Céline; Lamont - Doherty Earth Observatory Columbia University Karabulut, Hayrullah; Bogazıcı University, Geophysics
Keyword:	North Anatolian Fault, Propagation of a fault, Subduction, Extension, Aegea

SCHOLARONE™  
Manuscripts

1                                   **Propagation of a strike-slip plate boundary**  
2                                   **within an extensional environment :**  
3                                   **the westward propagation of the North Anatolian Fault.**

4

5    *Xavier le Pichon<sup>1</sup>, A. M. Celâl Şengör<sup>2,3</sup>, Julia Kende<sup>4</sup>, Caner İmren<sup>5</sup>,*  
6    *Pierre Henry<sup>4</sup>, Céline Grall<sup>6</sup> and Hayrullah Karabulut<sup>7</sup>*

7

8

9    <sup>1</sup> Professeur Honoraire au Collège de France, Europôle de l'Arbois, Bât. Trocadéro, BP 80  
10   13 545 Aix-en-Provence cedex 04 FRANCE

11   <sup>2</sup> İstanbul Teknik Üniversitesi, Maden Fakültesi, Jeoloji Bölümü, Ayazağa 34469 İstanbul  
12   TURKEY

13   <sup>3</sup> İstanbul Teknik Üniversitesi, Avrasya Yerbilimleri Enstitüsü, Ayazağa 34469 İstanbul,  
14   TURKEY

15   <sup>4</sup> CEREGE, CNRS-Aix Marseille Université, Marseille, FRANCE

16   <sup>5</sup> İstanbul Teknik Üniversitesi, Maden Fakültesi, Jeofizik Bölümü, Ayazağa 34469  
17   İstanbul, TURKEY

18   <sup>6</sup> Lamont - Doherty Earth Observatory Columbia University, Marine Geology and  
19   Geophysics, New York City, UNITED STATES

20   <sup>7</sup> Kandilli Rasathanesi, Boğaziçi Üniversitesi, Kandilli, İstanbul, TURKEY

21

22

23 ***Abstract***

24

25 The Sea of Marmara marks a key point in the propagation of the North Anatolian Fault  
26 (NAF) toward the northern extremity of the Aegean subduction during the last 12-11  
27 Myr. There is no indication that a localized plate boundary existed to the west of it, north  
28 of the Aegean portion of the Anatolia plate, before 2 Ma. Prior to 2 Ma, the shear  
29 produced by the motion of Anatolia-Aegea with respect to Eurasia was distributed over  
30 the whole width of the Aegean-West Anatolian western portion. This was most probably  
31 related to the presence there of a N/S component of extension produced by the  
32 southward migration of the Aegean-West Anatolian subduction. Fast subduction of the  
33 oceanic Ionian lithosphere had been initiated 15 Ma ago, a few million years before the  
34 Anatolia westward motion began 11 Ma ago. These two processes are obviously tightly  
35 linked. We document the establishment of the Aegea-Anatolia/Eurasia plate boundary in  
36 Plio-Pleistocene time in this geodynamic context.

37

38 We show that the beginning of the formation of a localized plate boundary occurred  
39 between 4.5 and 3.5 Ma ago at the location of the present Sea of Marmara by the  
40 initiation of a shear zone comparable to the Gulf of Corinth one in Central Greece. Thus  
41 the first part of the formation of the Sea of Marmara was purely extensional. We discuss  
42 the transition from the initial extensional basins to the present strike-slip system, that  
43 today cuts across the whole Sea of Marmara and that is called Main Marmara Fault  
44 (MMF). We show that the beginning of its development is not earlier than 2.5 Ma ago.  
45 Shortly after, the plate boundary migrated west of the Sea of Marmara along the  
46 northern border of Aegea from the North Aegean Trough, to the Gulf of Corinth area and

47 to the Kefalonia fault. There, it finally linked with the northern tip of the Aegean  
48 subduction zone, completing the system of plate boundaries delimiting the Anatolia-  
49 Aegea plate. We have related the remarkable change in the distribution of shear over the  
50 whole Aegea from Miocene to Pliocene to the formation of a relatively undeforming  
51 block in Pliocene that forced the shear to be distributed over a narrow plate boundary to  
52 the north of it. We attribute the formation of this relatively undeforming Aegean block to  
53 the northeastward progression of the cold oceanic Ionian slab. We propose that the slab  
54 cuts the overlying lithosphere from asthenospheric sources and induces a shortening  
55 environment over it.

56

57 ***Keywords***

58 North Anatolian Fault, Propagation of a fault, Subduction, Extension, Aegea, Anatolia

59

60 ***Introduction***

61

62 McKenzie (1970, 1972) first described the westward extrusion of Anatolia-Aegea in  
63 terms of plate tectonics, following Ketin's pre-plate tectonics suggestion in 1948. GPS  
64 results have confirmed that one could describe the Anatolian extrusion to a first  
65 approximation in terms of rigid rotations (Le Pichon et al. 1993, 1995; McClusky et al.  
66 2000, 2003; Reilinger et al. 1997; Reilinger et al. 2006; Le Pichon and Kreemer 2010).  
67 The northern boundary of this plate separates the Anatolia-Aegea plate to the south  
68 from the Eurasia plate to the north and is presently characterized along its whole 2100  
69 km length by dextral strike-slip at a rate of about 24 mm/yr. To the east, the portion of  
70 the boundary north of Anatolia corresponds to the 1200 km North Anatolian Fault  
71 (NAF) that propagated westward since 13-11 Ma (Şengör et al. 2005). The NAF reached  
72 the Gulf of İzmit in the Sea of Marmara about 4 Ma ago (Le Pichon et al. 2014) although  
73 shear related deformation in the broader Marmara region had already commenced in  
74 the late Miocene (Şengör et al. 2005). (See figure 1 for the tectonic map of Aegea-  
75 Western Anatolia in figure 1 and figure 2.5 as a key to geographic and geologic features  
76 in the Marmara area.) To the west, (see fig.1), the additional 900 km of plate boundary  
77 are complex (Şengör 1979; Şengör et al. 1982; Goldsworthy et al. 2002; Armijo et al.  
78 2002; Le Pichon and Kreemer 2010; Shaw and Jackson 2010; Floyd et al. 2010; Royden  
79 and Papanikolaou 2011; Pérouse et al. 2012). The plate boundary follows successively  
80 from east to west the NAF in the Sea of Marmara, called Main Marmara Fault by Le  
81 Pichon et al. (2001), the Ganos fault, the North Aegean Trough (NAT) formed by the  
82 Saros Basin to the east and the Sporades Basin to the west, followed by a broad zone of  
83 shear called the Grecian Shear Zone (GSZ) by Şengör (1979) to finally join through the

84 dextral Kefalonia Fault the Aegean subduction zone, where the 200 Ma Ionian oceanic  
85 slab is subducted at a rate of 34 mm/yr (Pérouse et al. 2012).

86

87 The central theme of this paper concerns the mode of establishment of such a strike-slip  
88 plate boundary since 13-11 Ma when the Aegea-Anatolia plate was first initiated. We  
89 attempt to understand better why a localized pure strike-slip fault has progressively  
90 propagated westward as emphasized by Şengör et al. (2005). An essential character of  
91 both Anatolia and Aegea is that their geological history suggests very thin or even absent  
92 lithospheric mantle (e.g. Şengör 1982). Thus the Aegea-Anatolia plate corresponds to a  
93 huge ductile mass. Further the western Aegean portion is subject to N/S extension  
94 because of the roll-back of the peri-Aegean subduction (Le Pichon and Angelier 1981; Le  
95 Pichon 1982). The ductility of this lithospheric mass and the presence of an important  
96 N/S extensional component on its western Aegean portion will occupy a prominent  
97 place in our investigation of the formation of this plate boundary. The transition from  
98 the well-defined NAF to the east to the more complex Aegean boundary to the west  
99 occurs within the Sea of Marmara. We will devote the principal part of this paper to a  
100 discussion of the genesis of the Sea of Marmara, as it enlightens the mode of propagation  
101 of the NAF through it. We will use new data and interpretations that have been partly  
102 published by Grall et al. (2012; 2013), Le Pichon et al. (2014) and Şengör et al. (2014) or  
103 are still unpublished (Kende, in preparation).

104

105 ***The present tectonic regime of the North Anatolian Fault and its***  
106 ***mechanical behavior***

107

108 ***The portion of the NAF east of the Sea of Marmara***

109 We first examine the behavior of the NAF east of the Sea of Marmara. The NAF there,  
110 throughout its length, is a stable localized pure dextral strike-slip fault with only local  
111 pull-apart and push-up segments (Şengör et al. 2005). The rate of geological motion has  
112 been established at about 18 mm/yr (18 over 10 kyr by Hubert-Ferrari et al. 2002, 18.6  
113 over 3 kyr by Kozacı et al. 2009 and 15 to 20 mm/yr in a compilation made by Kozacı et  
114 al. 2009). This rate is about 75% of the geodetic slip rate which suggests that 25% of the  
115 displacement is taken outside of the main fault plane, presumably along minor faults on  
116 both sides of it.

117

118 We wish to emphasize an important point concerning the temperature structure of the  
119 upper lithosphere along the NAF. This is illustrated by the variation in the Curie Point  
120 (580°C for magnetite) depth as mapped by Aydın et al. (2005) in their figure 4. The NAF  
121 follows the 20 km depth contour of the Curie Point. Immediately to the south, the Curie  
122 Point depth rises to less than 10 km. **Thus, the lower crust and mantle are highly**  
123 **ductile to the south of the fault and much less to the north where the NAF keeps its**  
124 **course.** The mapping of Aydın et al. (2005) demonstrates that the NAF keeps north of  
125 the boundary of the ductile lower crust and mantle zone. *This observation leads us to*  
126 *propose that the North Anatolian Fault (NAF) would not stabilize unless the whole crust is*  
127 *in the brittle domain. Otherwise, it has no roots and rapidly loses its "memory".* Geologists  
128 have long indicated that the geological history of Anatolia suggests that no lithospheric  
129 mantle is present there (e.g. Şengör 1982). One can thus understand why the attempts to  
130 enter the bulk of Anatolia, by the Ovacık and Sungurlu faults, were unsuccessful and why  
131 the NAF has followed the northern limit of this ductile mass.

132

133 ***The NAF in the Sea of Marmara***



134 Le Pichon et al. (2001) showed that the prolongation of the NAF within the Sea of  
135 Marmara, which they called the MMF, is a single throughgoing dextral strike-slip fault  
136 system that enters the Sea through the Gulf of İzmit and joins the Ganos fault at its  
137 western extremity. The geological slip rate along the eastern Çınarcık portion of this  
138 fault has been established to be 18.5 (12.6–29.4, 18.5 preferred rate) mm/yr over 500  
139 kyr by Kurt et al. (2013). Grall et al. (2013) found a rate of 15.1 to 19.7 mm/yr over 405-  
140 490 kyr to the west on the Western High (see fig.2.5). On the Ganos fault Aksoy (2009)  
141 found 15.1 to 19.7 mm/yr over 20 kyr and Meghraoui et al. (2012)  $17 \pm 5$  mm/yr over  
142 1000 yr. Thus the geological slip rate across the Sea of Marmara is about 18 mm/yr as  
143 on the main eastern portion of the NAF. The NAF motion is consequently integrally  
144 transferred from the North Anatolian Fault to the Ganos Fault through the MMF. As for  
145 the NAF to the east of the Sea of Marmara, the rate along the MMF is also about 75% of  
146 the geodetic slip rate which suggests again that 25% of the displacement is taken  
147 outside of the main fault plane.

148

149 Many authors have assumed the continuity of the rate of motion at the entrance of the  
150 Sea of Marmara. They consequently consider that the motion along the NAF there is  
151 distributed between a Marmara branch and a Gemlik branch to the south (see fig. 2.5).  
152 For example, Gasperini et al. (2011) have measured a strike-slip rate of 4 mm/yr on the  
153 southern branch. Should these 4 mm/yr be deducted from the 18 mm/yr on the eastern  
154 NAF to obtain the rate of the MMF? Le Pichon et al. (1999) pointed out that this would  
155 be true only if the block between the two branches, which they called the Marmara  
156 block, had the same motion as the Anatolia block, which would be most unlikely. If the  
157 Marmara block has an independent motion, then the motion of this block can be  
158 adjusted in such a way that the rate is the same on the eastern NAF and the MMF to

159 avoid any velocity discontinuity which would be otherwise mechanically very difficult to  
160 sustain. This is indeed what was found by Meade et al. (2002), Le Pichon et al. (2003),  
161 Reilinger et al. (2006), Le Pichon and Kreemer (2010) and other authors since, who have  
162 introduced in their GPS solution an independent Marmara block.

163

164 Note however that Gasperini et al. (2011) have measured average rates of about 9  
165 mm/yr on the NAF in the Gulf of İzmit by measuring offsets of a river channel that was  
166 drowned about 10 Kyr ago. This is about half the geological slip rate found to the east on  
167 the NAF and to the west in the Çınarcık Basin. This discrepancy is puzzling.

168

169 It is remarkable that the MMF follows the same 20 km Curie Point limit along the  
170 northern edge of the Çınarcık Basin as along the eastern NAF. The portion of the MMF  
171 that follows the northern border of the Çınarcık Basin within the eastern Marmara Sea  
172 corresponds to a stable localized strike-slip fault (Karabulut et al. 2002; 2011; Bulut et  
173 al. 2009; Örgülü 2011; Kurt et al. 2013). While the MMF is entirely contained within the  
174 thickly sedimented deep Marmara Basin, another fault system called South Marmara  
175 Fault by Le Pichon et al. (2014) was active in Pliocene time over the whole less  
176 sedimented southern shelf of the Sea of Marmara. Some activity is still related to this  
177 southern fault system. On the southern edge of the İmralı Basin, (Armijo et al. 2002)  
178 have described an active extensional system connected to the NAF in the Gulf of İzmit by  
179 a right-lateral fault along the shore of Armutlu Peninsula. Current fault activity does not  
180 seem continuous along the SW, transtensional, edge of İmralı Basin (see fig.2.5) but a  
181 number of active normal faults appear to distribute the extensional component of strain  
182 within the basin (Şengör et al. 2014). Moreover, subsidence at the depocenters proceeds  
183 at a steady rate since 0.4 Ma at least (Sorlien et al. 2012). Although little seismic activity

184 is recorded in this area, it is possible that the growth of the İmralı Basin may still today  
185 accommodate some significant strain.

186

187 The MMF crosses the 20 km Curie Point limit west of Çınarcık, as it changes direction to  
188 the WSW toward the Ganos Fault, to enter a hot lower crust and upper mantle area  
189 (Aydın et al. 2005). By doing so, it also enters into the serpentinite and mélange-  
190 dominated Intra-Pontide suture, which may also affect the mechanical behavior of the  
191 fault (see esp. Le Pichon et al. 2014, fig. 1b). There, in the western and central Sea of  
192 Marmara, this localized strike-slip fault appears to coexist with remnants of an  
193 extensional system, as demonstrated by significant distributed extensional seismic  
194 activity to the south of it (Altınok and Alpar 2006; Karabulut, unpublished data, 2015).  
195 This western portion of the MMF is thus best understood as an intermediate type of  
196 boundary, where a localized strike-slip fault has just been established within a  
197 previously existing broad zone of shear affecting the ductile lower crust and upper  
198 mantle.

199

#### 200 ***The NAF west of the Sea of Marmara***

201 From the Ganos fault westward into the Gulf of Saros, the Curie Point depth increases  
202 again to more than 20 km and the Ganos-Saros Gulf fault is indeed a stable pure strike-  
203 slip portion which corresponds to the westernmost extent of the stable pure strike-slip  
204 NAF (Karabulut et al. 2006). Recently the Mw 7.0 May 24 2014 earthquake confirmed  
205 the pure dextral strike-slip nature of the fault along the Saros Basin, all the way to 25°E  
206 (Görgün and Görgün 2015). Gasperini et al. (2011) using the same approach as in the  
207 Gulf of İzmit confirmed the existence of dextral strike-slip along the Saros fault. However  
208 they evaluated the rate as only about 10 mm/yr over the last 10 kyr post-glacial period.

209 This discrepancy with the geodetic slip rate of 22 to 24 mm/yr (Le Pichon and Kreemer  
210 2010; Pérouse et al. 2012; Müller et al. 2013) is similar to the discrepancy in the Gulf of  
211 İzmit and suggests that there might be some systematic bias in their evaluation.  
212 Moreover, we pointed out earlier that trenching studies estimate slip rate on Ganos fault  
213 at  $17\pm 5$  mm/yr (Meghraoui et al., 2012; Aksoy et al., 2009) over similar periods of time.

214

215 We conclude that the rate of dextral strike-slip motion is indeed constant from the NAF  
216 to the western extremity of the Gulf of Saros fault along the prolongation of the NAF at a  
217 geodetic slip rate of about 24 mm/yr. However, as discussed above, although the  
218 geological slip rate also appears to be constant at about 18 mm/yr, it is only about 75%  
219 of the geodetic slip rate. We proposed earlier that this discrepancy between geodetic  
220 and geologic rates may indicate that about 25% of the displacement is taken outside of  
221 the main fault plane.

222

223 ***The western portion of the North Anatolian Fault: the undeforming Aegea block, the***  
224 ***Ionian slab and the two shear zones that limit it***

225 We now move westward within the Aegean domain. A remarkable result established by  
226 the geodetic surveys of Aegea is the existence of an essentially undeforming Aegea block  
227 limited by two shear zones (Reilinger et al. 2006; Floyd et al. 2010; Le Pichon and  
228 Kreemer 2010; Royden and Papanikolaou 2011; see fig.1). The northern shear zone, as  
229 mentioned above, has been called Grecian Shear Zone (GSZ) by Şengör (1979, 1982). It  
230 absorbs about 20 - 25 mm/yr of dextral slip. To the east, the Western Anatolian Shear  
231 Zone (WASZ) absorbs about 20 mm/yr of sinistral slip. Both zones are characterized by  
232 distributed extension across several extensional asymmetric rifts with decollement,

233 accompanied by rapid rotation at about  $5^\circ/\text{Myr}$ , clockwise for the dextral GSZ and  
234 counterclockwise for the sinistral WASZ (see detailed references below).

235

236 The rates of rotation mentioned above of about  $5^\circ/\text{Myr}$  should be detected by  
237 paleomagnetic measurements if they persevered over several million years. Such  
238 rotations have indeed been detected (Kissel et al. 2003; Van Hinsbergen et al. 2005; Van  
239 Hinsbergen et al. 2010). They are clockwise in the western Aegean region and may have  
240 reached as much as  $40^\circ$  between 15-13 and 8 Ma with an additional  $10^\circ$  after 4 Ma (Van  
241 Hinsbergen et al. 2005). They are counterclockwise within the eastern Aegean region in  
242 the WASZ and have been measured as about  $20^\circ$  between 16 and 5 Ma (Van Hinsbergen  
243 et al. 2010). These finite rotations thus qualitatively agree with the present geodetic  
244 rotations. Of course, paleomagnetic techniques can only detect rotations of relatively  
245 short radius. The absence of detectable paleomagnetic rotations thus does not imply the  
246 absence of important motions of large rotation radius. In addition, as the paleomagnetic  
247 results are obtained by an averaging process between different sites, the distinction  
248 between local block rotations and regional rotations is difficult to make, especially in  
249 Aegea where numerous local block rotations have been demonstrated to be present.  
250 However, an important point is that the rapid phase of rotation detected by  
251 paleomagnetism began about 15-13 Ma to the west and 16 Ma to the east confirming that  
252 middle Miocene was an important time for the tectonics of Aegea.

253

254 The existence of this undeforming Aegea block is not integrated in recent discussions of  
255 the geodynamics of the area (e.g. Royden and Papanikolaou 2010; Vassilikis et al. 2011;  
256 Tirel et al. 2013; Pearce 2015). These recent discussions assume rapid lithosphere  
257 extension related to the subduction of the oceanic Mediterranean lithosphere since

258 Middle Miocene. But actually, the episode of rapid extension within the present Aegea  
259 block peaked between Serravallian, about 12 Ma ago, and Messinian (7 to 5 Ma) and  
260 ceased to exist within this Aegea block after Messinian time (5 Ma) while it continued  
261 within the WASZ and was initiated within the GSZ between 2 and 1 Ma ago (Armijo et al.  
262 1996; Sorel 2000; Flotté 2003). We attribute this cessation of extension within the  
263 present Aegea undeforming block to the shielding effect of the cold oceanic Ionian slab.  
264 The subduction of the Ionian oceanic slab started about 10 Ma ago and this shielding  
265 effect thus progressively extended over the whole southern Aegean mostly after  
266 Miocene time. Moreover, the slab now dips some 10° to 15° up to a distance of some  
267 300 km from the Hellenic "Trench". Despite the prodigious amounts of Messinian salt  
268 probably going down into the subduction channel, this would induce a considerable  
269 frictional stress onto the upper plate that would counteract the extension farther north  
270 in a situation not too different from the south-central Andes in Chile (see Oncken et al.  
271 2006, especially fig. 16-12 a-f). This would explain why the "dead" block does not extend  
272 far into the north in the Aegean Sea. Another explanation proposed by Sonder and  
273 England (1989) is that the thinning of the southern Aegean Sea that was initiated about  
274 20 Ma ago may have reached a critical level 3–5 Ma ago because of the cooling of the  
275 extending lithosphere, and that consequently the strain associated with the pull toward  
276 the arc was transferred further outward, including to western Anatolia. However, their  
277 proposal does not explain why the extension continued within northern Aegea and  
278 Western Anatolia although the extension had started at about the same time there. We  
279 will come back to this important point later on.

280

281 We now consider more carefully these two shear zones. *We will show that within the*  
282 *West Anatolian-Aegean domain, outside of the presently undeforming Aegea block, the*

283 *normal mode of shearing there, in this ductile lower crust-upper mantle environment, is*  
284 *through rotation of en-echelon normal faults over a 100-200 km wide shear zone*  
285 *(McKenzie and Jackson 1983, 1986, 1989; Jackson and McKenzie 1989). Further, the brittle*  
286 *distension roots in a shallow decollement above the ductile lower crust. This is because, in*  
287 *addition to the ductility of the lower crust and mantle below 10-15 km as in Eastern*  
288 *Anatolia, the thinned lithosphere is also affected by strong N/S extension due to the roll-*  
289 *back of the peri-Aegean subduction.*

290

291 The GSZ consists of several extensional rifts oblique to the direction of motion of Aegea  
292 with respect to Eurasia, the largest of these being the Corinth and Evia grabens (see  
293 fig.1). These are asymmetric rifts with active decollements (Rigo et al. 1996; Jolivet et al.  
294 2010). In this area, distributed extension is accompanied by rapid clockwise motion at  
295 about 5°/Myr (Le Pichon and Kreemer 2010; Floyd et al. 2010; Chousianitis et al. 2010).  
296 The width of this portion of the shear zone in a direction perpendicular to the motion of  
297 Aegea with respect to Eurasia is about 100-200 km. There is no localized strike-slip  
298 boundary there, as evidenced by the absence of strike-slip earthquakes. Yet, Durand et  
299 al. (2014) have suggested that there is a localized strike-slip boundary at depth, within  
300 the ductile portion of the lithosphere. The existence of shallow dipping decollements  
301 flattening at a depth of about 10 km suggests that the lower crust is ductile (Jolivet et al.  
302 2010). Further, Tiberi et al (2001) have shown that the Moho topography is unrelated to  
303 the surface tectonics as the lower crust appears to have been affected by boudinage. This  
304 confirms that the lower crust is most probably ductile there. Thus, there is no reason to  
305 assume the existence of a hidden extension of the NAF at depth below the CHSZ as  
306 proposed by Durand et al. (2014). Most authors had previously recognized the absence

307 of a localized strike-slip boundary at depth, notably Şengör (1979) and Goldsworthy et  
308 al. (2002).

309

310 The WASZ also consists of actively extending asymmetric rifts rotating counterclockwise  
311 at about 5°/Myr (Floyd et al. 2010). Karabulut et al. (2013) have put into evidence  
312 “small-amplitude and long-wavelength lateral variations of the Moho topography” which  
313 suggests to them that “viscous flow in a hot lower crust has smoothed out the lateral  
314 variations of crustal thickness.” Aydın et al. (2005) have shown that the Curie Point is at  
315 a depth of 5 - 10 km in this area, which confirms that the lower crust is indeed in the  
316 ductile regime. The width of the WASZ is similar to the width of the GSZ and equal to  
317 about 100-200 km. This width, of the order of the thickness of the average lithosphere,  
318 suggests that it is related to block shearing of the whole lithosphere. The deformation in  
319 the upper brittle crust is an adjustment to this underlying distributed shear. In  
320 conclusion, both the WASZ and the extensional portion of the GSZ have a similar width  
321 of about 100-200 km and have a hot and ductile lower crust. The underlying mantle is of  
322 course also hot and ductile. We can conclude that this type of shearing zone with  
323 rotating distributed extension in the upper crust is preferred in this extensional hot  
324 environment where the lower crust and upper mantle are ductile.

325

326 We then move to the two portions of the northern Aegean boundary that have not yet  
327 been discussed, on both sides of the GSZ: the Sporades Basin, at the western extremity of  
328 the North Aegean Trough to the east of the GSZ, and the Kefalonia-Patras fault system to  
329 the west. We show that these are portions of the North Aegean Boundary intermediate  
330 in character between stable pure strike-slip localized faults and highly distributed  
331 extension through rotating faults on top of a sheared lower crust and upper mantle. The



332 Sporades Basin appears to possess a localized strike-slip fault as well as distributed  
333 extension to the north of it (the Thermaikos and Chalkidiki extensional systems). The  
334 Kefalonia-Patras fault system has a major strike-slip fault at its northern extremity, the  
335 Kefalonia fault, and a minor one at its southern extremity, the Patras fault, with  
336 distributed shear in-between. Both portions of boundary appear to be sheared over a  
337 width of 100 to 200 km at depth in the lower crust and upper mantle.

338

339 A new insight on the behavior of these two portions of the boundary is given by the  
340 seismic sequence that followed the January 6 2008 Mw 6.2 earthquake (37.15°N,  
341 22.95°E). This earthquake ruptured the Ionian slab at a depth of 80 km (see Durand et  
342 al. 2014) and resulted first in roll-back of the subduction with southwestward motion of  
343 the top block toward the trench and then in dextral shear of Aegea with respect to the  
344 Eurasia plate. On June 8 1968, an Mw 6.4 dextral strike-slip earthquake activated the  
345 Patras-Achaïa strike-slip fault over a length of 25 km and then during the second part of  
346 2008, the GSZ (Corinth, Sperchios and Evia rifts) was activated in extension. This  
347 extensional activity extended northward into the NAT area within the Thermaikos and  
348 Chalkidiki extensional systems.

349

350 We now consider the velocity field across the GSZ. Floyd et al. (2010) show that both  
351 across the extensional part of the GSZ and across the Kefalonia and Patras-Achaia fault  
352 system, there is a continuous linear increase in GPS velocity with respect to Eurasia from  
353 about 5-10 mm/yr north of the Aegea block to 30-35 mm/yr within the block. This  
354 increase occurs over about 100-200 km, the gradient being somewhat steeper in the  
355 purely extensional area than in the Kefalonia-Patras strike-slip area (see also Shaw and  
356 Jackson 2010). The increase in velocity over more than 100 km cannot be explained only

357 by elastic effect because this width is too large. The only reasonable explanation is that it  
358 reflects ductile shear in the underlying mantle below, as concluded by Shaw and Jackson  
359 (2010) and Floyd et al. (2010).

360

361 Considering more carefully the Kefalonia-Patras shear system, the most important fault  
362 is the Kefalonia fault that absorbs about 15 mm/yr of dextral slip (Vassilakis et al. 2011)  
363 or up to 23 mm/yr (Pérouse et al. 2012). It links the northern extremity of the Aegean  
364 subduction to the Aegean northern boundary. As a consequence, the whole Kefalonia-  
365 Patras shear area lies on top of the shallow African slab that is subducted at a velocity of  
366 about 34 mm/yr, much faster than the 4 mm/yr convergence velocity of the Adriatic  
367 crust with the northern Greece crust, north of the Kefalonia fault (Pérouse et al. 2012).  
368 The lithosphere being sheared is everywhere thinner than about 50 to 40 km (Pearce  
369 2015). This is a very peculiar situation. We will come back to this point later when  
370 discussing the possible role of the slab. Cocard et al. (1999) had shown that this domain  
371 had an important clockwise rotation rate centered on the islands of Kefalonia and  
372 Zakintos. The rate of rotation is estimated at 6-8°/Myr by Chousianitis et al. (2014) and  
373 8°/Myr by Vernant et al. (2015). This Patras-Achaia area is limited to the northeast by a  
374 zone of left-lateral shear between the Gulf of Amavrakikos and the eastern tip of the Gulf  
375 of Corinth. The rate of motion along this zone of shear is estimated to be about 10  
376 mm/yr (Vassilakis et al. 2011; Vernant et al. 2015).

377

378 The June 8 2008 earthquake activated the Patras-Achaia fault at the southern extremity  
379 of the Kefalonia-Patras shear system as Durand et al. (2014) have demonstrated. This  
380 fault is identified by Shaw and Jackson (2010) through its seismicity but only appears on  
381 GPS as a change from a gradient in velocity to the north versus a uniform velocity to the

382 south. Vassilakis et al. (2011) tried to evaluate its motion by identifying small more or  
383 less rigid "fragments" and conclude that the motion is 7 mm/yr with about 5 mm/yr in  
384 extension and 5 mm/yr in strike-slip. This is not in agreement with the pure strike-slip  
385 motion revealed by the June 8 earthquake. In any case, their method maximizes the  
386 motion on the boundaries between blocks as it ignores any internal deformation. Thus  
387 one can only state with certainty that the motion along this fault is too small to be  
388 properly characterized by GPS. Indeed, the fault cannot be identified on the field (Shaw  
389 and Jackson 2010). Cases of faults with strong seismogenic potential but too small slip  
390 rate to be detected by geodetic methods have indeed been described elsewhere (e.g.  
391 Friedrich et al. 2004). Thus the Kefalonia-Patras shear area is a zone of continuous shear  
392 deformation over a width of at least 100 km bounded by two localized strike-slip faults.  
393 The most important is the Kefalonia fault that absorbs about 20 mm/yr of dextral slip  
394 (15 mm/yr for Vassilakis et al. 2011, 20 mm/yr for Vernant et al. 2015 and 23 mm/yr  
395 for Pérouse et al. 2012). The Patras-Achaïa fault absorbs a maximum of about 5 mm/yr.  
396 The June 2008 earthquake activated it, as Durand et al. (2014) have demonstrated.

397

398 We now go back to the NAT. Although Reilinger et al. (2006), Le Pichon and Kreemer  
399 (2010), Pérouse et al. (2012) and Müller et al. (2013) all agree that dextral strike-slip at  
400 a rate of 22 to 26 mm/yr occurs along the NAT, the presence of simultaneous active  
401 extension immediately to the north of the Sporades Basin in the Thermaikos and  
402 Chalkidiki extensional systems indicates that the western NAT does not correspond to  
403 pure strike-slip localized on a single fault. Pérouse et al. (2012) and Müller et al. (2013)  
404 emphasized this point. The activation of the Sporades and Chalkidiki extension, but not  
405 of the Sporades dextral strike-slip, during the 2008 seismic sequence confirms that this  
406 is an intermediate type of boundary, where a localized strike-slip fault coexists with

407 remnants of an extensional system, on top of a broad zone of shear affecting the ductile  
408 lower crust and upper mantle. We have seen above that this intermediate type of  
409 environment also characterizes the central and western Marmara Sea with simultaneous  
410 presence both of a localized strike-slip fault, the MMF, and of active remnants of the  
411 previous extensional system.

412

413 To conclude, west of the Saros Basin, the northern boundary of the Aegean block  
414 absorbs 22 to 24 mm/yr of dextral strike-slip over a broad 100-200 km wide zone of  
415 shear of the lithospheric mantle, with various expressions within the upper crust. From  
416 east to west, there are first both localized strike-slip along the Sporades Basin and  
417 simultaneous extension to the north in the Thermaikos and Chalkidiki area. Then there  
418 is distributed clockwise rotating extension within the GSZ. Finally, there is distributed  
419 shear between two strike-slip faults, the Kefalonia and Patras-Achaïa faults in the  
420 westernmost portion. This last portion joins the northern boundary of the Anatolia-  
421 Aegea plate to the Aegean subduction plate boundary. It crosses an area of relatively  
422 thin crust with no well identified Moho, on top of the shallow subducting slab (Pearce  
423 2015). The crust there probably consists of geologically recent stacks of cold nappes cut  
424 from the asthenosphere by the underlying slab as discussed by Pearce (2015). This  
425 relatively cold environment accounts for the presence of localized strike-slip faults.

426

427 *It is important to note that the effect of the deformation in the GSZ and WASZ is to allow*  
428 *the relatively undeforming Aegea block to rotate clockwise away from Anatolia around a*  
429 *pivot situated near the northern extremity of the subduction zone (see for example figure 8*  
430 *of Le Pichon and Kreemer 2010, in which the GPS vectors are with respect to Anatolia).*

431 This rotation has two effects on the subduction zone. First, it increases the subduction

432 rate to a value of about 35 mm/yr along the whole NW/SE segment of the Hellenic  
433 subduction zone as this rotation compensates for the southeastward decrease of motion  
434 of the Anatolia/Eurasia rotation. Second, it maintains the subduction direction strictly  
435 perpendicular to the subduction zone (Le Pichon and Angelier 1979). This rotation thus  
436 appears to be governed by the roll-back of the subduction zone.

437

#### 438 ***Consequences of the subduction of the Ionian slab***

439 Coming back to the drastic consequences of the subduction of the cold and heavy  
440 oceanic Ionian slab, *we argue that the presence of a low dip cold slab in rapid subduction*  
441 *has drastic consequences for the overlying mantle and crust. This is because it cuts the*  
442 *overlying lithosphere from asthenospheric sources and induces a shortening environment*  
443 *over it. This, in our opinion, explains why major extension is absent within the present*  
444 *Aegea block while it was very active between 13 and 5 Ma.*

445

446 The cold 200 Ma old oceanic Ionian slab (Truffert et al. 1993) is presently subducted  
447 below Aegea at a velocity of about 34 mm/yr, much faster than the 4 mm/yr  
448 convergence velocity of the continental Adriatic crust north of the Kefalonia fault with  
449 the northern Greece crust (Pérouse et al. 2012). The length of the seismically active slab  
450 is about 350 km below Peloponnesus (e.g. Gudmundsson and Sambridge 1988), which  
451 indicates that this rapid subduction is 10 Myr old or somewhat older if the average rate  
452 of subduction since the initiation of subduction was equal or somewhat smaller than the  
453 present one. The volcanic arc related to this subduction was initiated near 2.5 Ma (Le  
454 Pichon and Angelier 1979). The slab below the volcanic arc is about 150 km deep and  
455 the length of slab from the volcanic arc to the subduction zone is about 300 km. Thus the  
456 age indicated for the initiation of subduction is also 10 Ma or somewhat older.

457

458 This age is in fair agreement with the age of formation of the accretionary wedge, which  
459 occurred after 15 Ma as established by deep sea drilling (Kastens et al. 1991). Located  
460 within a trough near the backstop leading edge, DSDP 377 borehole penetrated early to  
461 middle Miocene (between 19 and 15 Ma) turbidites of probable African origin. At the  
462 time the turbidites were deposited, the present accretionary wedge could not have  
463 existed if the turbidites indeed came from Africa. These turbidites were covered with 15  
464 to 14 Ma pelagic marls whereas turbidites continued to be deposited to the south. Thus  
465 the change of sedimentation to pelagic marls at 15 Ma is compatible with an initiation of  
466 the present accretionary wedge at about this time. The probable limestone backstop is  
467 covered by late Miocene basins confirming that it reached its present configuration also  
468 in the late Middle Miocene, near 15 Ma (Le Pichon et al. 2002). Thus this margin was  
469 formed approximately 15 Ma ago. Le Pichon et al. (2002) proposed that this was a time  
470 of reinitialization of the subduction system after slab break. We adopt their proposal.  
471 This late initiation of the Ionian oceanic plate would also explain why the Kefalonia  
472 transform is geologically quite recent (post-Messinian, 5-7 Ma according to Royden and  
473 Papanikolaou 2011). We have noted above that the finite clockwise and  
474 counterclockwise rotations detected by paleomagnetism within Aegea were initiated 16  
475 to 15 Ma.

476

477 The alternative is that the slab stops being seismically active 10 Myr after being  
478 subducted but continues at greater depth as an aseismic slab. This alternative is  
479 proposed by authors who postulate continuity of the slab to great depth on the basis of  
480 tomographic studies (Bijwaard et al. 1998; Piromallo and Morelli 2003). In this line of  
481 thought, Royden and Papanikolaou (2011) and Tirel et al. (2013) agree that rapid

482 subduction of the cold Ionian lithosphere would only have started at 6-8 Ma, following a  
483 slower subduction episode of external carbonate platform on transitional lithosphere.  
484 However, in their hypothesis, it is hard to understand how the slab was able to maintain  
485 its continuity as it went from oceanic in Eocene time, to semi-continental in Oligocene  
486 and lower to middle Miocene, then back to oceanic again in upper Miocene to Recent  
487 time. Models that have been proposed to investigate the change due to the subduction of  
488 a continent (Martinod et al. 2000; Royden and Husson 2006) suggest that continental  
489 subduction induces an increase in the slab dip angle and a decrease in the subduction  
490 velocity due to a change in slab buoyancy. They also predict that the slab should break at  
491 the former location of the continental block. These models then are difficult to reconcile  
492 with the interpretations, which assume continuity of the slab and no break, such as  
493 those proposed by Tirel et al. (2013) and Pearce (2015).

494

495 The relationship between simple idealized 2-D models of subduction and actual 3-D  
496 complex Aegean subduction is not obvious. For example, the continental subduction  
497 north of the Kefalonia transform dips at the same 17° shallow angle as the oceanic  
498 subduction to the south (Pearce 2015). However the assumption of a 200-300 km  
499 narrow Ionian slab extending uninterrupted over more than 1000 km in spite of these  
500 drastic changes in subduction type and subduction direction is based on tomography.  
501 But is the assumption justified? The presumed continuous slab depicted by tomography  
502 shows significant heterogeneity (see fig. 7c of Bijwaard et al. 1998, and section Ff of  
503 figure 9 of Piromallo and Morelli 2003). More importantly, the continuity is undermined  
504 by the proven existence of slab breaks in its upper portion. A major slab break, long  
505 suspected on the basis of tomographic studies, has been demonstrated to exist between  
506 Aegea and Anatolia (Paul et al. 2014). Pearce (2015) concludes his extensive

507 investigation of seismic imaging of the western Hellenic subduction by stating that  
508 “there may be two overlapping slabs beneath northern Greece, one dipping at 17°  
509 toward N60°E from 30 to 70 km depth and the other sitting horizontally at 200 km  
510 depth”, as shown by Soboudi et al. (2006). He also indicates that he cannot exclude a  
511 tear of the slab between northern and southern Greece as proposed by Spakman et al.  
512 (1993) and concludes that the slab may be locally segmented in some way at least near  
513 its top. The existence of these ruptures conforsts the conclusion of Le Pichon and  
514 Kreemer (2010) who pointed out that the continuity of the conical seismic slab with a  
515 deeper slab could not be maintained without significant rupture.

516

517 Furthermore, the extent of the Ionian slab below Aegea, as defined by the intermediate  
518 seismicity distribution (Gudmundsson and Sambridge 1988; Shaw and Jackson 2010), is  
519 broadly confirmed by the high-resolution surface tomography of Salaün et al. (2012),  
520 which shows that the low-velocity anomaly in the upper mantle, between 80 and 160  
521 km depth, present in Anatolia and north central Aegea, is limited to the south by the  
522 seismically active Ionian slab. Paul et al. (2014) show that the zone of low velocity  
523 anomaly, in Anatolia and north central Aegea, has NE/SW fast-wave polarization axes of  
524 shear-wave anisotropy, whereas in southern Aegea, where the seismically active slab is  
525 present, the orientation is quite different and significantly smaller.

526

527 The mapping of intermediate seismicity depth in the slab by Gudmundsson and  
528 Sambridge (1988) and Shaw and Jackson (2010) confirms that the slab is not present  
529 below the Corinth and Evia grabens, although Suckale et al. (2009) assume that the slab  
530 extends below the eastern extremity of the Corinth Gulf beyond a depth of 100 km.  
531 However, this assumption of Suckale et al. (2009) does not appear to be substantiated.



532 This is because their composite images of the slab show that the well-defined image of  
533 the slab disappears at a depth of 100 km before reaching the area below the eastern Gulf  
534 of Corinth. The mapping of Gudmunsson and Sambridge also indicates that the slab is  
535 present below the Kefalonia-Patras shear zone, as discussed above. And the detailed  
536 seismic imaging of the western Hellenic subduction by Pearce (2015) confirms the  
537 presence of the slab below the Kefalonia-Patras shear zone, as noted earlier. We can  
538 conclude that the slab is absent below the GSZ and present below the Kefalonia-Patras  
539 zone, which would explain the tectonic difference below the two zones.

540

541 Note that the continuity-of-slab hypothesis also leads to another difficulty as it does not  
542 explain why the extensional collapse of the Aegean landmass, which resulted in the  
543 formation of the Sea of Crete, could have occurred above a shallow subducting slab that  
544 should have created a compressional environment. Drooger and Meulenkamp (1973)  
545 have shown that the Southern Aegean landmass fragmented and most of it came below  
546 sea level at the end of Serravallian (about 13 Ma, see also Angelier 1979) while it is now  
547 part of the undeforming Aegean block since Messinian, at about 5 Ma (Angelier et al.  
548 1982). We submit that the apparent heterogeneity of the tomographic slab may be due  
549 to the coalescence of pieces of slab following various tear episodes in Late Eocene and  
550 Middle Miocene.

551

552 If this tear of the slab did indeed occur prior to the initiation of subduction of the oceanic  
553 Ionian slab between 15 and 10 Ma, one can then distinguish between the presently  
554 subducting Ionian slab at a rate of 34 mm/yr and with a dip of  $17^\circ$  toward N35°E  
555 reaching a maximum depth of 170 km and the older coalesced slabs now dipping at  
556 about  $45^\circ$  toward the north between 170 km and about 1200 km (Bijwaard et al. 1998).

557 This older system, which extends over 1000 km and penetrates into the lower mantle, is  
558 most probably anchored within the mantle. Consequently its kinematics are  
559 independent of what happens at the surface. Its vertical velocity must be approximately  
560 equal to the vertical component of velocity of the subducted Ionian slab, so that contact  
561 is maintained between the two subducted pieces. Thus the vertical velocity of the Ionian  
562 slab is about 10 mm/yr. This vertical velocity implies an age of the order of 100 Ma for  
563 the initiation of subduction of this older slab, which is quite reasonable.

564

565 We consequently conclude that the subducted Ionian slab now prevents the  
566 asthenosphere from reaching the base of the lithosphere and produces above it a  
567 tectonic environment that is cooler and affected by shortening, or at least much less  
568 extension. We argue that this is the reason why the essentially undeforming Aegea block  
569 coincides with the part of Aegea that is presently underlain by the Ionian slab. This then  
570 explains why the Sea of Crete, that resulted from the extensional collapse of the Aegean  
571 landmass during Mid to Late Miocene, when a slab was absent below it, following the  
572 post-Oligocene break, has been part of the undeforming Aegean block since Messinian,  
573 about 5 Ma ago (Angelier et al. 1982). At this time, the Ionian slab began to propagate  
574 northeastward below the Sea of Crete and consequently cut off the asthenospheric  
575 source on which this extension thrived.

576

577 ***The penetration of the NAF within the western-Anatolian-Aegean***  
578 ***landmass 4 Ma ago***

579

580 Figure 2 shows our proposed reconstruction of the NAF 4 Ma ago. Le Pichon et al. (2014)  
581 have shown that at this time the NAF had not yet entered the area of what is now the Sea

582 of Marmara but had just reached its eastern extremity, near the Gulf of İzmit. We will  
583 show that this is the time at which asymmetric extensional rifts similar to those of the  
584 present Gulf of Corinth were formed in the southern part of what is now the Sea of  
585 Marmara. These rifts were oblique to the direction of motion of Anatolia with respect to  
586 Eurasia, with active decollements to the south of a large anticline on the present  
587 southern shelf of the Sea of Marmara. This distributed extension, which we consider to  
588 have been accompanied by rapid clockwise motion, accommodated the deformation on  
589 the western tip of the 4 Ma NAF (Fig. 2, 3a and 3b).

590

591 Let us first briefly discuss the geodynamics of the western-Anatolian-Aegean landmass 4  
592 Ma ago. We have seen that the present geodynamics of Aegea and the prolongation of  
593 the NAF along its northern boundary are now greatly influenced by the presence of the  
594 rapidly subducting Ionian slab. This is because the subduction of the slab resulted in the  
595 formation of an undeforming Aegean block on top of the advancing slab. This subduction  
596 was initiated about 15 Ma ago, 3 to 4 Myr before the NAF initiated its westward  
597 propagation (12 to 11 Ma ago according to Şengör et al. 2005). The fact that subduction  
598 of the oceanic Ionian plate immediately preceded the formation of the NAF suggests that  
599 slab pull was essential to trigger the extrusion of Anatolia. Before the slab had  
600 sufficiently advanced to result in the formation of the relatively undeforming Aegean  
601 block, between 15 and 4 Ma ago, the Western Anatolia-Aegea environment was  
602 dominated by ductile lower crust and upper mantle and was affected by strong N/S  
603 extension due to the roll-back of the peri-Aegean subduction distributed over the whole  
604 Aegean. **In this tectonic environment, the shear between the westward motion of**  
605 **Anatolia and Eurasia was distributed over the whole width of Aegea. As a**

606 **consequence, there was no localized northern boundary fault north of Aegea**  
607 (Fig.2).

608

609 This does not mean that extension was not present in the northern Aegean. For example,  
610 the North Aegean Trough has deposits of Messinian (7-5 Ma) evaporites (Mascle and  
611 Martin 1990) and Messinian carbonates and marls are present along the coasts of Saros  
612 Gulf and Çanakkale close to North Aegean Trough (Çağatay et al. 1998, 2006; Melinte-  
613 Dobrinescu et al. 2009). But there was no localized zone of shear along it. However as  
614 the Ionian slab progressed northeastward below Aegea, distension ceased within the  
615 overlying lithosphere and a relatively undeforming Aegean block progressively  
616 increased its size. Consequently, the shear could not be distributed over the whole of  
617 Aegea. Accordingly, the kinematics had to adjust and a localized zone of shear began to  
618 form along the northern boundary of Aegea. This is confirmed by the fact that the age of  
619 the GSZ is quite young, less than 2 Ma. Armijo et al. (1996) have shown that the phase of  
620 rapid extension in the Gulf of Corinth corresponds to the last million years and Sorel  
621 (2000) and Flotté (2003) have dated the initiation of the Gulf of Corinth between 1.7 and  
622 1.1 Ma. Flotté (2003) estimated the total extension to be 15 km. This finite extension  
623 should be compared to the present rate of extension of 15 mm/yr. It is equivalent to 1  
624 Myr of extension at the present rate. Nielsen (2003) estimated the dextral offset along  
625 the Kefalonia fault at 37 km using the offset of two portions of a seamount that appeared  
626 to have been cut in two pieces. This offset would have been produced in 1.6 Myr using  
627 the strike-slip rate of 23 mm/yr given by Pérouse et al. (2012). Similarly, Tüysüz et al.  
628 (1998) estimated the age of the initiation of dextral motion in the Gulf of Saros as  
629 between 2 and 1 Ma, Kurt et al. (2000) as Plio-Quaternary and Ustaömer et al. (2008) as  
630 Quaternary. This strike-slip phase followed a compressional phase in the Saros Gulf

631 region (4-3 Ma) based on the age of the Conkbayırı Formation, an alluvial fan formed on  
632 the uplifted southern shoulder of Saros Gulf (northern Gelibolu Peninsula) (see e.g.,  
633 Sümengen et al. 1987; Çağatay et al. 1998). *Thus the present northern plate boundary of*  
634 *Aegea is less than about 2 Ma from the Gulf of Saros to the Kefalonia fault.*

635

636 We should remember however that the 200 km WASZ had been a zone of active  
637 extension since Late Miocene and remained in this situation to this day. Consequently  
638 the prolongation of the NAF within the Sea of Marmara, which is situated exactly to the  
639 north of the WASZ, can be considered to be a leaky transform. The Sea of Marmara thus  
640 marks a major transition in the propagation of the NAF toward the Aegean subduction  
641 zone.

642

#### 643 ***The Pliocene Sea of Marmara***

644 We now return to the area that will become the Sea of Marmara about 4 Ma ago. Le  
645 Pichon et al. (2014) described a continuous gently curvilinear, south-concave zone of  
646 deformation about 10 km wide that extended over the whole southern shelf of the Sea of  
647 Marmara, from the Gulf of Gemlik to the Dardanelles Strait, in Lower Pliocene time,  
648 about 4 Ma (Fig. 3a and 3b). They called this zone of deformation the South Marmara  
649 Fault (SMF) system and proposed that the SMF was then a branch of the dextral North  
650 Anatolian Fault. They noted that this zone of deformation was associated with a large  
651 anticline within the central part of the section, between Marmara and İmralı islands  
652 (Fig.3a, 3b and 3c). However the anticline was not found west of Marmara Island nor  
653 east of İmralı Island and the reason for the association of the anticline with the central  
654 part of the SMF was not elucidated in their paper.

655

656 The basement in the anticline area has been uplifted by more than 1 km, forming a 6 to  
657 10-km-wide anticlinal fold. The consequent uplift led to the erosion of the upper  
658 sedimentary units near the summit of the anticline. This folding occurred as the  
659 uppermost SE dipping foreset beds of the Alçitepe formation (uppermost Miocene–  
660 Lower Pliocene, 5.3 to 3.7 - 3.4 Ma, Melinte-Dobrinescu et al. 2009) were still being  
661 deposited to the south of the present southern shelf of the Sea of Marmara. The source of  
662 the sediments during their deposition was to the NW and not to the south, which  
663 indicates that the Sea of Marmara deep basins did not exist then. Both the upper  
664 Miocene (Kirazlı, 11-10 to 5.3 Ma) and Uppermost Miocene - Lower Pliocene (Alçitepe)  
665 sedimentary sequences were conformably deposited, then folded and strongly eroded  
666 (Fig. 3c and 4). Le Pichon et al. (2014) concluded that the uplift occurred near the end of  
667 Lower Pliocene, between approximately 4.5 and 3.5 Ma. The uplift of the basement  
668 increases westward toward Marmara Island and the maximum uplift is about 1.5-2 km  
669 over Marmara Island that was uplifted and broadly warped at this time (see Le Pichon et  
670 al. 2014 for a short discussion of the tectonics of the island). An examination of the  
671 topography of the island confirms the broad EW anticlinal upwarp of the island. We  
672 reexamined the termination of the anticline west of the island of Marmara for this paper  
673 (fig.4). The anticline and the uplift terminate abruptly along a NNW/SSE normal fault  
674 west of the island of Marmara.

675

676 Le Pichon et al. (2014) noted that the SMF occupies the apex of the anticline. But the  
677 SMF continues westward of Marmara island to the Biga Peninsula, just east of the  
678 Dardanelles Straits, whereas the anticline does not. If the anticline and the SMF were  
679 cogenetic, the disappearance of the anticline west of Marmara Island would be puzzling  
680 as one would expect the shortening component to increase as the SMF bends its

681 direction southwestward west of Marmara. Indeed the SMF is clearly compressional  
682 west of the island of Marmara and, during the Pliocene, a compressional regime  
683 prevailed in the north of the Gelibolu Peninsula, with the formation of the Anafartalar  
684 thrust and the deposition of the Conkbayırı alluvial fan related to it (e.g., Çağatay et al.  
685 1998). However, the anticline along the SMF disappears west of the Island of Marmara,  
686 thus this folding appears to be not contractional. This suggests that the formation of the  
687 anticline is not related to the SMF. We can conclude further that the SMF occupied the  
688 apex of the anticline immediately after the anticline was deactivated, probably because  
689 the apex was the weakest portion of the crust as Steckler and ten Brink (1986) predicted  
690 that, within a zone of continental thinning, a strength minimum exists just seaward of  
691 the hinge zone. But the activity of the SMF was geologically brief as it was terminated  
692 when Lower Pliocene fresh water calcareous mudstones were deposited, probably  
693 corresponding with the Conkbayırı Formation.

694

695 We propose that the anticline is related to a phase of extension comparable with the one  
696 now occurring within the GSZ in the Gulf of Corinth and we relate it to the detachments  
697 mapped by Bécél et al. (2009) in the southern Sea of Marmara between the sea floor and  
698 13 km depth (see figures 3a, 3b and 3c). We also show in figures 3a and 3b the crests of  
699 tilted blocks on top of these detachments as mapped by Bécél et al. (2009). To illustrate  
700 the similarity between this system and the Gulf of Corinth extensional system, we show  
701 in figure 5 an interpreted lithospheric SW-NE profile (see location on figure 6). The fault  
702 locations are from Le Pichon et al. (2014) and Laigle et al. (2008) and the supra-crustal  
703 model is based on Bayrakci et al. (2013) while the detachment geometry comes from  
704 Bécél et al. (2010). The Moho depth is the Kende et al. (in prep.) model and will be  
705 discussed later when presenting figure 6. Interpretation of seismic profiles of Turkish

706 Petroleum (TPAO) were also consulted to constrain the fault and sediment deposition  
707 geometries on the southern shelf. The locations of microearthquakes are from Kandilli  
708 Observatory data. We have added in figure 5, below the profile, the sketch of Jolivet et al.  
709 (2010) that illustrates the possible future evolution of the Gulf of Corinth to illustrate  
710 the similarity between this structure and the Gulf of Corinth one. The possible evolution  
711 of the Gulf of Corinth described by Jolivet et al. (2010) is that of a typical Cordilleran-  
712 style metamorphic core complex. The origin of the antiform has been attributed to the  
713 footwall isostatic rebound by many authors since Spencer (1984) and Wernicke et al.  
714 (1985). We consider that figure 5 demonstrates that the Southern Shelf anticline and the  
715 decollement of Bécél et al. (2009) are cogenetic. Because we know the age of formation  
716 of the anticline, about 4 Ma, we conclude that the area corresponding to the southern  
717 portion of the present Sea of Marmara was similar to the present Gulf of Corinth about 4  
718 Ma.

719

720 In figures 3a, 3b and 3c, the anticline has two distinct portions, a Marmara portion to the  
721 west and an İmralı one to the east. They both have the same orientation and the same  
722 width. But they appear to be left-laterally offset. We have sketched in dotted line along  
723 the direction of this offset a possible shear. A similar shear with the same direction  
724 might limit the İmralı anticline portion and separate it from the Armutlu uplift. Finally,  
725 another one might limit the western extremity of the İznik Basin. In the tectonic context  
726 of the time, these shears might correspond to left-lateral x shears and be related to the  
727 clockwise rotation that must have affected the whole area in front of the western tip of  
728 the NAF, rotation which is attested by the clockwise rotation of  $16^\circ$  detected  
729 paleomagnetically by Avşar and İşseven (2009) on volcanic Eocene rocks of the Armutlu  
730 Peninsula. It is interesting to note in this context that the orientation of the large İmralı



731 canyon is compatible with the direction of these probable x-shears. But we do not have  
732 enough structural data to identify this other possible İmralı canyon x-shear. Note  
733 however that, as noted above, the fault along the western end of Armutlu Peninsula has  
734 been interpreted by Armijo et al. (2002) as being presently an active dextral fault  
735 limiting the presently extending İmralı Basin.

736

737 The presence of the İmralı portion of the anticline led us to investigate whether it could  
738 also be associated with a detachment, similar to the Marmara one, to the west of the  
739 Armutlu Peninsula. We noted on the SEISMARMARA seismic profile in the İmralı Basin,  
740 shown in fig 2.b of Laigle et al. (2008) (see location of the profile in figures 3a and 3b),  
741 that the basement dipping northward could be interpreted as a detachment and the  
742 basement between İmralı and Çınarcık as a huge tilted block. As we had no other  
743 information, we gave to this detachment the same orientation as the Bécel et al. (2009)  
744 detachment. We converted it into depth following the conversion used by Bécel et al.  
745 (2009). This double basin interpretation, i.e. a western one (paleo-Central basin) and an  
746 eastern one (paleo-İmralı Basin), leads us to propose that the whole area corresponding  
747 to the present Sea of Marmara was occupied about 3.5 to 4.5 Ma by two asymmetric  
748 extensional basins, with detachments dipping NNE, within a broad zone that rotated  
749 clockwise in front of the tip of the advancing NAF, as depicted schematically in figure 2.  
750 This area then should correspond to the oldest portion of the Sea of Marmara and  
751 should have a purely extensional origin.

752

753 An intriguing point is that the western anticline segment increases in amplitude  
754 westward toward Marmara Island, whereas the eastern one increases in amplitude  
755 eastward toward İmralı Island. This opposite polarity would be expected if these basins

756 formed a relay between the Eastern NAF and a just initiated paleo-Ganos-Gulf of Saros  
757 Fault. This situation then would be similar to the present situation of the GSZ as a relay  
758 between the NAT and the Kefalonia-Patras Fault system (see figure 16 of Shaw and  
759 Jackson 2010).

760

761 Figure 6 shows the present distribution of the marine Alçitepe Formation and of the  
762 continental Pliocene after the map of the General Directorate of Mineral Research and  
763 Exploration (2002), Görür et al. (1997) and Sakıncı et al. (1999). This is the first time  
764 when marine Mediterranean and the Marine Paratethyan sequences began mixing in the  
765 later history of the Marmara Sea and the well-controlled shape of the marine ingression  
766 indicates that it was the southern fault systems that were governing the route of the  
767 invading seas (see especially Figs. 9 and 10 in Sakıncı et al. 1999). The distribution of the  
768 Alçitepe neritic formation in the west corroborates that the basins, formed between  
769 approximately 4.5 and 3.5 Ma, were situated in the southern portion of the present Sea  
770 of Marmara. The distribution of the formations to the west of the present Sea of  
771 Marmara appears to be compatible with the initiation of a paleo-Ganos-Gulf of Saros  
772 Fault during Uppermost Miocene – Lower Pliocene.

773

774 We conclude that sometime between 4.5 and 3.5 Ma, two left-laterally offset basins were  
775 formed in a purely extensional context and now correspond to the oldest part of the  
776 present Sea of Marmara. At the end of this tectonic episode, the NAF entered for the first  
777 time in the Marmara area, through the present Gemlik Bay, within what would later  
778 become the shelf of the Sea of Marmara, following the axis of the İmralı and Marmara  
779 anticlines. It then presumably joined a paleo-Ganos-Gulf of Saros Fault. Le Pichon et al.  
780 (2014) named this branch of the NAF the South Marmara Fault. Note that, in our

781 interpretation, the present Gemlik fault was part of the early SMF. Thus, we propose that  
782 the SMF was the primary structure in Pliocene and that prior to Pliocene, the shear was  
783 distributed over the whole western Anatolia. There was no primary structure then.

784

785 The formation of the SMF marked the end of the initial extensional phase and the  
786 beginning of the second strike-slip phase, although the transition between the two  
787 stages was most probably gradual because extension is still present today in the  
788 southern part of the Sea of Marmara. During this second phase, the strike-slip motion  
789 migrated northward and established itself along the present MMF. It was responsible for  
790 the architecture of the northern part of the Sea of Marmara, which was submitted to a  
791 strikingly different strike-slip context than the one prevailing during the first purely  
792 extensional phase.

793

#### 794 ***Crustal thinning below the Sea of Marmara***

795 Before getting into the discussion of this second mostly strike-slip phase of formation of  
796 the Sea of Marmara, we need to examine crustal thinning there in the context of the  
797 overall thinning prevalent in Aegea and Western Anatolia since Middle Miocene. Crustal  
798 thinning has been investigated by different means with consistent results over the  
799 Whole Aegean -Western Anatolian area (e.g. Tiberi et al. 2001; Tirel et al. 2004;  
800 Karabulut et al. 2013; Pearce 2015). The crust has been systematically thinned by more  
801 than 10 km below the Aegean Sea (Tirel et al. 2004; Pearce 2015) as well as below the  
802 Sea of Marmara (Bécel et al. 2009; Karabulut et al. 2013), the GSZ (Tiberi et al. 2001)  
803 and the WASZ (Karabulut et al. 2013). The shallowest Moho is found at a depth of 24 km  
804 below the NAT, 23-24 km beneath the Sea of Crete (Tirel et al. 2004) and 23-24 km  
805 below the GSZ (Tiberi et al. 2001). In the latter case, Tiberi et al. (2001) pointed out that

806 the highest Moho point is offset with respect to the Gulf of Corinth. This offset suggested  
807 to them that the lower crust is affected by boudinage. Below the WASZ, Karabulut et al.  
808 (2013) observed long-wavelength variations of Moho depth, from about 25 km below  
809 the Sea of Marmara (in agreement with Bécel et al. 2009) to about 32 km beneath the  
810 İzmir–Ankara suture and to about 25 km beneath the Menderes Massif. This long-  
811 wavelength variation suggested to these authors that viscous flow in a hot lower crust  
812 has smoothed out the lateral variations of crustal thickness, as mentioned earlier.

813

814 *This brief review indicates that the overall crustal thinning in Aegea –Western Anatolia*  
815 *has proceeded locally to maxima that lifts the Moho to a depth of about 25 km, below the*  
816 *Gulf of Corinth, northern Aegea, the Sea of Crete, the Sea of Marmara and the WASZ. This*  
817 *value of 25 km is too prevalent to be purely coincidental. It affects regions where thinning*  
818 *started at widely diverse ages between 20 and 2 Ma. We suggest that this depth of about*  
819 *25 km of Moho corresponds to the stage of thinning at which the gravitational potential*  
820 *energy of the Aegean continental lithosphere, with respect of the potential energy of the*  
821 *adjacent Ionian oceanic lithosphere, reaches its minimum value (see discussion for*  
822 *example in Le Pichon 1982). Thus, from that stage on, the thinning can only propagate*  
823 *laterally outward. These results suggest furthermore that the lower crust has a long-*  
824 *term viscous mechanical behavior, with boudinage deformation, during the thinning*  
825 *process, as mentioned earlier.*

826

827 These important remarks will guide us in the following discussion of the thinning  
828 process below the Sea of Marmara in which we will use a new Moho model developed by  
829 Kende et al. (in prep, see Annex). Kende et al. (in prep.) selected 30 km for the depth of  
830 Moho corresponding to an absence of thinning. This value of 30 km is the one given by

831 Karabulut et al. (2013). We preferred it to the 35 km given by Bécel et al. (2009) as they  
832 have few constraints away from the offshore domain and as their 35 km value does not  
833 seem compatible with the model of Karabulut et al. (2013) although we note that their  
834 N-S 2D model spreads the thinning on a larger area than in our model. Our resulting  
835 Moho depth model shown in figure 7 maps the Moho depth below the whole Sea of  
836 Marmara. The Moho is shallowest at two locations, one north of Marmara Island and the  
837 other southwest of the Çınarcık Basin, with a smooth variation in between. The largest  
838 amount of crustal thinning there is about 10 km. The western zone of highest thinning is  
839 narrower and impinges on the southern shelf whereas the eastern one is wider and  
840 occupies the whole width of the Çınarcık Basin. We note further that the thinning under  
841 the Sea of Marmara is asymmetric, steeper to the north and more gradual to the south.  
842 Below the MMF, the Moho depth is remarkably constant near 26 km (see figure 10f that  
843 will be discussed later). It deepens abruptly to more than 29 km as the fault leaves the  
844 Sea of Marmara, both to the east and the west. The maximum thinning is situated about  
845 10 km to the south of the MMF in the western Marmara Moho high and about 15 km to  
846 the south of the MMF in the eastern Çınarcık Moho high. In between, near the profile  
847 shown in figure 5, the maximum thinning coincides with the MMF. The asymmetry is  
848 clearly seen on the profile of figure 5 and appears to reflect the asymmetry of the  
849 decollement mapped by Bécel et al. (2009). This suggests that the development of the  
850 deep crustal structure of the Sea of Marmara has been controlled by the two initial  
851 Alçitepe southern rifts. This control can also be seen in the dual nature of the zone of  
852 maximum thinning, which reflects the emplacements of the two Alçitepe rifts. The  
853 eastern Çınarcık Moho high corresponds to the paleo-İmralı Basin whereas the western  
854 Marmara Moho high corresponds to the paleo-Central Basin.

855

856 However, it is also striking that there is no one to one correlation between the upper  
857 crust structure and the lower crust and mantle one. For example, the zone of maximum  
858 thinning to the west extends below the island of Marmara. In addition, although one  
859 should be aware of the imperfect resolution of the Moho mapping that was used, the  
860 Moho topography is quite smooth, which suggests that the lower crust is indeed  
861 governed by a ductile rheology that allows it to flow on a geological time scale. We noted  
862 earlier that Karabulut et al. (2013) had used the smoothness of the Moho topography in  
863 Western Anatolia as an argument in favor of the flow of the lower crust. This change of  
864 rheology between upper and lower crust is also suggested in figure 5 by the  
865 confinement of the seismicity of the MMF to the upper crust. Thus the upper crust there  
866 appears to coincide with the brittle crust. We conclude that our investigation agrees  
867 with our previous discussion on the ductile nature of the lower crust and upper mantle  
868 over the Aegean-West-Anatolian area. Although the structure of the Moho topography  
869 below the Sea of Marmara appears to have been in great part controlled by the  
870 formation of the two Alçitepe extensional grabens, its evolution appears to be partly  
871 decoupled from the evolution of the upper crust. In addition, it must have been  
872 influenced by the later geological strike-slip phase, with the migration of the strike-slip  
873 fault northward to the present emplacement of the MMF and the formation of the more  
874 recent Tekirdağ and Çınarcık basins.

875

876 In figure 8 we compare the “Basement” topography after Bayrakci et al. (2013) to the  
877 topography of the Moho shown in figure 7. The “Basement” of Bayrakci et al. (2013)  
878 does not coincide everywhere with the crystalline basement. Basement in figure 8 is  
879 assumed to have a seismic velocity larger than 4.2 km/s. This is because they find a  
880 velocity step between 3.9 km/s and 4.5 km/s. It can be considered to be the layer on

881 which occurred the onset of sedimentation in the newly formed North Marmara Trough.  
882 The difference between the topography of the basement and the topography of the  
883 Moho is striking. Actually, at first sight, one does not see any significant correlation  
884 between the two topographies. However, a closer examination shows that the two E-W  
885 elongated deep basement troughs that are the main characteristic of the topography of  
886 the basement appear to be controlled by the two Alçitepe grabens. The eastern Çınarcık  
887 basement trough corresponds to the paleo İmralı-Basin whereas the western Tekirdağ-  
888 Central Basin basement trough is closely correlated to the paleo-Central Basin. But at  
889 the difference of the two Moho highs, the linear structure of the troughs follows the  
890 direction of the present MMF. The MMF lies at the axis of the western trough, whereas  
891 the MMF, which follows the base of the continental slope in the Çınarcık Basin, is parallel  
892 but offset 10 km to the north of the eastern trough.

893

894 It is remarkable that it would be impossible to predict the present topography  
895 characterized by three main basins, Çınarcık, Central and Tekirdağ, separated by two  
896 highs, Central and Western, on the basis of the topography of the basement! That one  
897 cannot predict the topography in such an area from the topography of the Moho is not  
898 surprising, in view of the decoupling effect of the ductile lower crust. But nobody, to our  
899 knowledge, expected the absence of correlation between the topography of the  
900 basement and the sea floor topography. This indicates that the two highs are structures  
901 that have no roots in the basement. Both highs thus are the products of sedimentary  
902 cover tectonics decoupled from the basement, most probably triggered by the strike-slip  
903 motion along the MMF. However, this remark needs to be qualified by the fact that the  
904 Central High is a zone where the crust is somewhat thicker than either east and west.

905

906 ***The evolution of the NAF in the Sea of Marmara from Lower Pliocene to***  
907 ***Present***

908

909 ***Age of onset of sedimentation in the newly formed North Marmara Trough***

910 To better understand the propagation of the NAF in the Sea of Marmara after the  
911 formation the Alçitepe dual-basins structure, we now try to evaluate our present  
912 knowledge of the age of the onset of sedimentation within the different parts of the Sea  
913 of Marmara. A synthetic map is presented in figure 9. This map reflects our still  
914 considerable uncertainties. We have chosen to classify the ages in four categories.

915

916 *The oldest basins, between 4.5 and 3.5 Ma* are those that were formed during the Alçitepe  
917 extensional stage discussed above. To the west, an onset age of 5 to 3.5 Ma in the South  
918 Central area was proposed on the basis of a heat flow model by Grall et al. (2012).  
919 Although this evaluation is fragile, it agrees with the 4.5-3.5 Ma that we proposed above  
920 for the basin produced during Alçitepe by extension along the Marmara decollement  
921 mapped by Bécel et al. (2009). We thus adopt an age of 4.5 to 3.5 Ma. This zone most  
922 probably extends further west to the western extremity of the Marmara anticline in the  
923 southern Tekirdağ Basin. To the east, in the North İmralı Basin, Sorlien et al. (2012)  
924 show a profile along a line north of the present depocenter in their figure 13. If one  
925 applies a constant rate of sedimentation and takes into account the effect of compaction,  
926 the basin in this zone should be at least 2 Ma. It is definitely older than the Çınarcık Basin  
927 to the north or the Tekirdağ Basin to the west. Having no stratigraphic constraints on  
928 the deeper horizons, we consider reasonable to assume that the age is the one predicted  
929 by the formation of the İmralı decollement and anticline between 4.5 and 3.5 Ma.



930 *The intermediate 2.5 to 1.5 basins* might correspond to the initiation of shearing along  
931 the MMF. A maximum age of 1.5 to 2.5 Ma has been proposed by Grall et al. (2012) for  
932 the Central Basinette. They show that if one assumes that the subsidence rates have  
933 been constant since the beginning of the formation of this basin, the age cannot exceed  
934 2.5 Ma. But although the rate of subsidence has been constant since 250-300 ka, a more  
935 rapid subsidence may have been present earlier, which would lead to a younger age. The  
936 heat flow model of Grall et al. (2012) confirms that this basin is younger than the basin  
937 in the South Central area. We assume for the Western High a similar age in view of the  
938 great thickness of sediment (Şengör et al. 2014; Bayrakci et al. 2013). This zone might  
939 extend all the way to westernmost Çınarcık (see discussion below)

940 *The youngest 1.5 to 1 Ma basins* correspond the Tekirdağ and Çınarcık basins. Seeber et  
941 al. (2004) proposed that the Tekirdağ Basin was created by oblique slip. They obtain a  
942 maximum age of 1.4 Ma with the parameters used in their model. We believe that if one  
943 takes into account the compaction, the maximum age may not exceed 1 Ma. Sorlien et al.  
944 (2012) and Kurt et al. (2013) used the same model to predict an age increasing from  
945 east to west in the Çınarcık Basin with less than 1 Ma for the easternmost Çınarcık and  
946 up to 1.4 in the central portion. We extrapolate an age of 1.5 to 2.5 Ma for westernmost  
947 part of Çınarcık. Note that the young age of the Çınarcık Basin suggests that the İzmit-  
948 Sakarya segment of the NAF that now enters the İzmit Bay is definitely younger than the  
949 İznik fault that enters the Gemlik Bay to the south.

950 *Figure 9 then is compatible with the existence of a southern Marmara basin formed*  
951 *between 4.5 and 3.5 Ma and a more complex composite younger northern Marmara basin*  
952 *that propagated outward to the east and to the west sometime after 2.5 Ma along the*  
953 *newly formed SMF.*

954

955 ***Subsidence along the MMF since 2.5 Ma***

956 In the following, we explore the possibility that since 2.5 Ma the northern Marmara  
957 basins along the present MMF developed through extension accommodated mostly by  
958 oblique slip on the transform fault itself (Seeber et al. 2004, 2006; Sorlien et al. 2012;  
959 Kurt et al. 2013). Such a model was originally proposed by Seeber et al. (2004) to  
960 explain the asymmetry and time-transgressive behavior characteristic of basins, such as  
961 the Tekirdağ basin, that form on the releasing sides of bends on strike-slip faults. The  
962 authors cited above have shown that this type of model is quite successful to account for  
963 the formation of the basins of the Sea of Marmara that are directly linked to the MMF, in  
964 particular the Tekirdağ at its western extremity and the Çınarcık at its eastern  
965 extremity. We apply the model through its simplest form. We assume that the side of the  
966 fault that is not subsiding is fixed and that the basement dip is parallel to the slip vector.  
967 Then the plunge (angle of slip motion with respect to the horizontal) of the slip vector  
968 along the main fault is the arc tangent of the subsidence velocity divided by the  
969 horizontal velocity. It is thus directly related to the subsidence rate through the rate of  
970 horizontal slip. This rather crude model is only used to test the general viability of a  
971 process of formation of the basins through extension mostly accommodated by oblique  
972 slip as discussed above.

973

974 To derive the plunge values presented in figure 10c we assumed a horizontal slip along  
975 the MMF of  $18 \pm 2$  mm/yr (Kurt et al. 2013; Grall et al. 2013) in agreement with the  
976 general discussion we had earlier on the geological slip rates along the NAF. The  
977 subsidence rates (figure 10b) were derived from various data discussed below.

978

979 Çınarcık: Kurt et al. (2013) presented a stratigraphic interpretation of the TAMAM dense  
980 grid of multichannel seismic profiles. The subsidence rates were derived from the  
981 difference between the depths of the green-H5 horizon, a seismic reflector described by  
982 Sorlien et al (2012) which age is estimated to be 540 - 630 ka [Sorlien et al. 2012; Grall  
983 et al. 2013], on each side of the fault. From the east, the subsidence rate decreases,  
984 starting at 5.5 - 4.7 mm/yr (Figures 3 and 4 in Kurt et al. 2013) to about 3.7 - 3.2 mm/yr  
985 in the middle part of the basin and 1.8 - 1.5 mm/yr to the west (Figure 3 in Kurt et al.  
986 2013), giving the corresponding plunge values of 17.1°, 11.6° and 5.9°. The 17.1° plunge  
987 value also corresponds to the dip of the basement along the fault at the eastern corner of  
988 the basin.

989

990 Kumburgaz: From the same TAMAM survey, Sorlien et al. (2012) presents a profile  
991 cutting the Kumburgaz Basin on its western part. Following the same method, a  
992 subsidence rate of 1.5 - 1.3 mm/yr and a 4.7° plunge is derived from the green-6  
993 (another seismic reflector described by Sorlien et al. 2012) depth variation of 0.8 km  
994 across the fault (Figure 11 in Sorlien et al. 2012).

995

996 Central Basin: Grall et al. (2012) presented two models of a profile cutting the basin: a  
997 steady-state model based on subsidence rate extrapolation and a model based on  
998 seismic line interpretation. We used the depth variation across the fault of the 2 Myr  
999 level in the first model and of the 1.5 Myr level on the second model as they are  
1000 presented in their supplementary material [Grall et al. 2012]. Both models yield the  
1001 same subsidence rate of 2 mm/yr and a plunge of 6.3°.

1002

1003 Western High: Grall et al. (2013) indicate a sedimentation rate over the last 39 kyr that  
1004 reaches a maximum of 1.5 mm/yr in the eastern and western small basins pinching in  
1005 the Western High (Figure 6 in Grall et al. 2013). Correcting for the compaction of  
1006 shallow sediment of 65-70% porosity, subsidence at crustal level at these sites should  
1007 account for about one third of the seafloor subsidence rate. This gives a subsidence rate  
1008 of 0.5 mm/yr corresponding to a plunge of less than 2° over the Western High.

1009

1010 Tekirdağ: The plunge values of 8° and 14° for, respectively, the Tekirdağ Basin and the  
1011 Ganos small basin off Ganos are inferred by Seeber et al. (2004) assuming that the  
1012 Tekirdağ Basin geometry is due to a stationary onset point, relatively to the south side of  
1013 the fault. Thus, the 8° plunge of the basin floor along the fault must correspond to the  
1014 fault plunge. For the Ganos small basin, Seeber et al. (2004) observed that the absence of  
1015 horizontal offset where the fault enters the basin could be explained by a displacement  
1016 plunge equal to the basin rim slope of 14°. Note that because the Tekirdağ Basin is  
1017 forming northward of the fault, the plunge values are considered as negative, as for the  
1018 Central Basin.

1019

1020 Moreover, we considered a relative subsidence equal to zero on average across the  
1021 Western High and on the Central High on either side of the Kumburgaz Basin. The  
1022 uncertainties were derived from values given in the cited studies, when available.  
1023 Consequently, most of them were calculated based on uncertainties on age models and  
1024 on horizontal slip rate (15 to 20 mm/yr) but do not take into account the uncertainty in  
1025 the relative vertical displacement.

1026

1027 The main interest of figures 10a and 10b is to illustrate the clearly anomalous nature of  
1028 the western Tekirdağ Basin and of the eastern Çınarcık Basin with their fast outward  
1029 propagation rate. There, the model proposed by Seeber et al. (2004) appears to account  
1030 in an elegant way for the evolution of these basins in a pure strike-slip mode. In-  
1031 between the rates are relatively modest and probably can be accounted for by simple  
1032 additional N/S distension which is known to be present because of its seismic signature,  
1033 especially to the south of the western and central part of the Sea of Marmara (Altınok  
1034 and Alpar 2006; Karabulut personal communication, 2015). We proposed earlier that in  
1035 the western and central Sea of Marmara, the MMF coexists with remnants of an  
1036 extensional system. Finally, as noted earlier, to the east, the active faulting and  
1037 subsidence in the İmralı Basin area may also involve continued activity on early  
1038 structures formed under extension.

1039

1040 Figure 10e shows the sediment thickness along the MMF after Bayrakci et al. (2013) and  
1041 confirms the very large thickness of sediment below the Western High, up to more than  
1042 6 km. We discussed this point earlier. Figure 10f gives the depth of the Moho from the  
1043 inversion of Kende et al. (in preparation) shown in figure 7. In figure 10d the crustal  
1044 thickness is obtained by subtraction of the bathymetry and sediment thickness from the  
1045 Moho depth. The constancy of the Moho depth along the MMF at about 26.5 km is in  
1046 contrast with the relatively large variation in the crustal thickness. This contrast again  
1047 testifies that the lower crust acts as a decoupling level in the structuration of the  
1048 Marmara area. We can also note that the overall thinning of the crust is relatively  
1049 modest.

1050

1051 To conclude, the evidence we have discussed is compatible with a two-stage formation

1052 of the Sea of Marmara. First, two left-laterally offset basins, a paleo-Central basin to the  
1053 west and a paleo-İmralı Basin to the east, were formed between 4.5 and 3.5 Ma, in a  
1054 purely extensional context, in front of the advancing NAF. They now correspond to the  
1055 oldest part of the present Sea of Marmara. The formation of the SMF on the southern  
1056 shelf marked the end of the initial extensional phase and the beginning of the second  
1057 strike-slip phase. During this second phase, the strike-slip motion migrated northward  
1058 and established itself along the present SMF. Sometime after 2.5 Ma, the northern basins  
1059 were formed along the present MMF through extension accommodated mostly by  
1060 oblique slip on the transform fault itself (Seeber et al. 2004, 2006; Sorlien et al. 2012;  
1061 Kurt et al. 2013). However the transition between the two stages has most probably  
1062 been gradual because extension is still present today, especially in the southern part of  
1063 the western and central Sea of Marmara as well as within the İmralı Basin.

1064

#### 1065 ***From extension to strike-slip***

1066 The evidence we have presented demonstrates, in our opinion, that the formation of the  
1067 Marmara deep basin began about 4.5 Ma during a 1 Myr purely extensional phase,  
1068 similar to the one producing today the Corinth rift. Furthermore, the evidence we  
1069 discussed above indicates that the proposition made by Le Pichon, Taymaz and Şengör  
1070 (2000) that the present MMF is a continuous dextral strike-slip fault which transfers the  
1071 slip of the eastern NAF from the Gulf of İzmit to the Ganos fault with a geological slip  
1072 rate of 18 mm/yr is correct. The question then is when did the tectonic change from  
1073 extension to strike-slip occur and how much finite motion corresponded to each of these  
1074 tectonic phases. This question does not have simple definitive answers today.

1075

1076 To approach this problem we may start from the total slip on the eastern branch of the

1077 NAF, which is estimated today at about  $75 \pm 10$  km (Şengör et al. 2005). This is  
1078 equivalent to 4.1 Myr of slip at the present geological slip rate of 18 mm/yr, much  
1079 smaller than the age of initiation of about 11 Ma. This led Şengör et al. (2005) to assume  
1080 a slip rate progressively increasing from zero 11 Ma to the present rate during the last  
1081 Myr. With their model, the total finite offset at the beginning of the purely extensional  
1082 phase in the Marmara area between 4.5 and 3.5 Ma is slightly more than 20 km and the  
1083 geological rate of slip at that time about 12 mm/yr. The modelization of Provost et al.  
1084 (2003) has demonstrated that the present NAF implies an extremely low friction  
1085 coefficient of less than 0.05 on the fault plane, fifteen times smaller than normal. Such a  
1086 low friction coefficient indicates that the principal displacement zone is well developed  
1087 and has reached its maturity through the effect of regularization by many successive  
1088 earthquakes, which would have produced a total offset of at least 20 km (e.g. Chester et  
1089 al. 1993). 20 km is probably the minimum amount of offset one may expect at this time  
1090 for the NAF to produce on its tip a well developed extensional shear zone. We accept this  
1091 20 km estimate of Şengör et al. (2005) for the offset at 4 Ma and the corresponding  
1092 probable rate of slip of 12 mm/yr at this time.

1093

1094 Note that this conclusion has an important consequence for the tectonics of Aegea from  
1095 Upper Miocene to Lower Pliocene. This is because, as a consequence, during this period,  
1096 the subduction rate must have been significantly less than today, probably not more  
1097 than 20 mm/yr as an average, with a progressive increase between 15-12 Ma and 4 Ma,  
1098 compared to the present subduction rate of 34 mm/yr.

1099

1100 We now move to the recent period of strike-slip. The formation of the Tekirdağ and  
1101 Çınarcık basins by the present MMF occurred at approximately the present 18 mm/yr

1102 geological slip rate since about 1.5 Ma. This indicates that about 27 km of total slip  
1103 occurred since 1.5 Ma on the MMF. We are left with approximately 30 km of total slip for  
1104 the period between 3.5 and 1.5 Ma. This gives an average rate of about 15 mm/yr,  
1105 which appears reasonable in view of the many uncertainties. The question then is how  
1106 this approximate amount of 30 km of total slip was distributed? What was the part of the  
1107 emerging MMF between 2.5 and 1.5 Ma, the part of possible intermediate systems of  
1108 strike-slip between the SMF and the MMF and the part absorbed in the still existing  
1109 extensional system? We do not have the information necessary to answer this. We can  
1110 only state with certainty that the present strike-slip system along the MMF was fully  
1111 functional at the present rate since 1.5 Ma.

1112

1113 Le Pichon et al. (2001) and Le Pichon et al. (2003) had been impressed by the  
1114 observation that the MMF cuts across older existing structures in the Sea of Marmara.  
1115 They concluded that the MMF appeared in a late stage of evolution of the Sea of  
1116 Marmara. Noting that back-slipping the MMF by 4 km appears to restore the Central  
1117 Bassinette to a symmetric shape, Le Pichon et al. (2001) concluded the MMF appeared  
1118 only about 200 ka. This estimate appeared to be reinforced by the discovery by Armijo  
1119 et al. (2002) of an offset of 3.5 km of a N/S fold on the Central High. This conclusion was  
1120 further elaborated by Rangin et al. (2004) and Şengör et al. (2005). It is clear now that  
1121 this interpretation was not correct and that the event that affected the MMF about 200  
1122 ka was probably a readjustment of the MMF (Grall et al. 2012). But this does not change  
1123 the observation that the MMF cut across the Marmara basin more than 2 Ma after its  
1124 initial extensional formation and that the structures related to it, such as the two  
1125 elongated basement troughs mapped by Bayrakci et al. (2013), are superimposed on an  
1126 older principally extensional framework.



1127

1128 ***Additional discussion of the geodynamics***

1129

1130 We pointed out throughout this paper that the lithospheric mantle of the Aegea-Anatolia  
1131 plate appears to be very thin or even absent and thus that the plate corresponds to a  
1132 huge ductile mass. This is because the Curie Point isotherm (580°C) south of the NAF is  
1133 nearly everywhere at a depth of less than 20km (Aydın 2005), which puts the  
1134 temperature at more than 900°C at the Moho. This Curie Point isotherm rises to less  
1135 than 10 km in southwestern Anatolia! McKenzie et al. (2005) have shown that, in  
1136 continental as well as oceanic lithosphere, the brittle seismogenic zone is limited at its  
1137 base by the 600°C isotherm. And numerous studies have confirmed that the part of the  
1138 mantle that is above 600°C does not contribute significantly to the elasticity of the plate.  
1139 As a consequence, the mantle in most of Anatolia and Aegea, south of the NAF, has  
1140 negligible mechanical resistance. Further, because the temperature within the lower  
1141 crust exceeds 750°C, many models predict that channel flow is possible if the  
1142 composition of the crust is not granulitic (e.g. Beaumont et al. 2004). In addition,  
1143 because partial fusion is prevalent in many places within the lower crust, transient  
1144 channel flow would appear as soon as the rate of partial fusion is sufficiently high  
1145 (McKenzie and Jackson 2002). We can conclude that the mechanical resistance of the  
1146 Aegean-Anatolian lithosphere lies essentially within its upper brittle crust and that  
1147 everything happens as if the lower crust acts as a decoupling level. The existence of a  
1148 decoupling level, somewhere within the lower crust or at the Moho, has been an  
1149 important acquisition of modern tectonics (e.g. Wernicke et al. 2008). The presence of a  
1150 decoupling level below the upper crust explains the observation we made earlier that  
1151 the NAF appears not to be able to stabilize unless the whole crust is in the brittle

1152 domain. If there is possible flow in the lower crust, the upper part of the fault is  
1153 disconnected from its roots and rapidly loses its "memory".

1154

1155 If the Aegean-Anatolian lithosphere is mechanically so weak, then how is it possible that  
1156 traction at its southwestern extremity can be transmitted over 1500 km to its eastern  
1157 extremity? The answer lies in the role played by the surface relief. The sometime  
1158 exclusive interest given to the role of the detachments of the slabs in the last few years  
1159 has led to a neglect of the very important role played by the evolution of topography,  
1160 with the notable exception of Floyd et al. (2010) for the Aegean-West Anatolian area.

1161 McKenzie (1972) and Le Pichon (1982) had both proposed that the westward  
1162 movement of the Anatolian lithosphere responded to a gradient in gravitational energy.  
1163 Currently the elevation of this plateau is about 2 km and the elevation regularly  
1164 decreases westward to below sea level within the Aegean Sea (see figure 11). The  
1165 existence of this westward slope of 1.5/1000 results in a gradient of potential  
1166 gravitational energy that enables the transmission of boundary forces to occur smoothly  
1167 over the whole length of the Anatolia-Aegea plate (see Le Pichon and Kreemer 2010 for  
1168 a more complete discussion of these dynamics). And this gradient explains how the  
1169 southwestward trench pull upon the Aegean lithosphere can lead to a westward traction  
1170 of Anatolia. But when and how was this gradient established?

1171

1172 Let us first consider when this gradient was established? There is a paradox there. The  
1173 last marine sediments deposited above the present East Anatolian Plateau date from  
1174 Serravallian, 13-11 Ma (Şengör et al. 2003). Thus the uplift started at this time, as  
1175 indicated by the volcanic activity, that was initiated 11 Ma and became plateau-wide at 8  
1176 Ma. Şengör et al. (2003) reasonably attributed part of the uplift of the East Anatolian

1177 Plateau to slab break-off, arguing that the asthenosphere appeared to lie immediately  
1178 below the crust, as evidenced by its anomalously low seismic velocity. The existence of a  
1179 slab break-off was also proposed by Faccenna et al. (2006) and by many others since, as  
1180 tomographic studies have demonstrated that the plunging African slab below Turkey is  
1181 detached from the African plate. But, during the same Serravallian time, most of what  
1182 now forms the central and southern Aegean Sea was rapidly subsiding. Drooger and  
1183 Meulenkamp (1973) have described the spectacular fragmentation of the southern  
1184 Aegean landmass that passed below sea level about 13 Ma. Yet, the Aegean Sea crust is  
1185 also underlain by hot asthenosphere (Salaün et al. 2012, Paul et al. 2014), as below the  
1186 East Anatolian Plateau. As discussed earlier, the subsidence there, in spite of the  
1187 presence of hot mantle, results from the fact that, during middle to late Miocene, the  
1188 crust of the Aegean Sea was thinned by more than 10 km.

1189

1190 Since the work of Aubouin et al. (1976), it has been demonstrated that after the  
1191 Paleogene phase of nappe stacking, the central Aegean had been the site of intense  
1192 crustal extension since the beginning of Miocene. This extension had formed core  
1193 complexes through uplift of the lower middle continental crust to the surface during the  
1194 middle to late Miocene (Lister et al. 1984). It seems reasonable to assume that the  
1195 present location of the core complexes were in late Oligocene to early Miocene the sites  
1196 of maximum crustal thickness and highest topography, and that they became the sites of  
1197 maximum crustal extension (Le Pichon et al. 2002). We have argued earlier that this  
1198 occurred because the Aegean portion of the slab broke, sometime in late Oligocene,  
1199 about 10 Myr earlier than below the East Anatolia Plateau. Consequently, at this time,  
1200 the asthenosphere rose to come in contact with the lower crust at the Moho. As its  
1201 southern boundary was a free boundary, able to migrate southward, the crust reacted by

1202 southward extension, whereas, 10 Myr later, below the East Anatolia Plateau, no  
1203 extension was possible because of the collision to the south at the Bitlis suture: the only  
1204 possibility was uplift. We thus had a situation in early Miocene in which the Aegean and  
1205 westernmost Anatolia were relatively high whereas the Eastern Anatolia Plateau was  
1206 close to sea level, the exact reverse of what it is now.

1207

1208 We now try to consider how the gradient was established. The topographic and crustal  
1209 thickness profiles in figure 11 indicate that there is a linear relationship between  
1210 topographic elevation  $h$  and crustal thickness  $T$ :  $h = (T - 27)/9.5$  in km. The crustal  
1211 thickness for sea level is 27 km and for an altitude of 2 km, on the plateau, 46 km. This is  
1212 to be compared to the relationship for Tibet,  $h = (T - 35)/7$  (Le Pichon et al. 1992). The  
1213 linear relationship demonstrates that a simple Airy type isostasy prevails there. The fact  
1214 that, to produce 1 km of additional elevation, one has 9.5 km of additional crustal  
1215 thickness in Anatolia-Aegea instead of 7 km in Tibet indicates a lower density contrast at  
1216 the Moho for Anatolia-Aegea than for Tibet. For example, using the values of upper crust  
1217 density of 2.67 and of lower crust density of 2.95, as adopted by Kende et al. (in  
1218 preparation), the density of the mantle would be 3.26 for Anatolia-Aegea and 3.39 for  
1219 Tibet. Of course, this model is very crude but it does confirm that the mantle below the  
1220 Moho is unusually light, and consequently hot, below Anatolia-Aegea.

1221

1222 If the thickening to 45 km of the crust below the East Anatolia Plateau can be explained  
1223 by crustal thickening north of the Arabian indenter, no such effect can be invoked to  
1224 explain the variation in thickness of the crust in central and western Anatolia. The only  
1225 process that we are able to invoke is lower crust flow from the East Anatolia Plateau  
1226 toward the west. Such a flow should actually be expected in view of the large of amount

1227 of magmatism since 8 Ma. This magmatism would have greatly decreased the viscosity  
1228 of the middle-lower crust (McKenzie and Jackson 2002). Actually, this tectonic situation  
1229 can be compared with what is now happening on the eastern border of the Tibetan  
1230 Plateau. This eastern border has been uplifted, without substantial shortening of the  
1231 upper crust, since 8 Ma, because of the occurrence of east-southeastward flow of the  
1232 middle-lower crust (e.g. Royden et al. 2008). We conclude that an eastward flow of the  
1233 lower crust of the East Anatolia Plateau has led to the progressive uplift of Anatolia from  
1234 east to west.

1235

1236 But was the mantle involved in this westward flow? We have argued that a level of  
1237 decoupling exists in Anatolia-Aegea within the lower crust. Consequently, the mantle  
1238 may not necessarily take part in this flow. However, the asthenosphere that had risen up  
1239 below the East Anatolia Plateau had to escape outward, being pushed by the advancing  
1240 Arabian indenter and the only possibility of escape for the asthenosphere was to the  
1241 southwest, toward the Mediterranean, between the Arabian indenter to the east and the  
1242 Aegean slab to the west. Do we have any indication that such a flow has existed? We can  
1243 again consider the Tibetan area where the orientation of the fast-wave polarization axes  
1244 of shear waves aligns itself with directions of principal shear indicating a flow in the  
1245 mantle, in the same direction as the surface one, with deformation rates exceeding 75%  
1246 (Holt 2000). On the southeastern border of the Tibetan Plateau, however, Flesch et al.  
1247 (2005) conclude that the mantle flow, as indicated by these polarization axes, is  
1248 probably decoupled from the crust. The eastward flow is actually close to the  
1249 extensional direction, at an angle with the southeastward surface flow, suggesting that  
1250 deformation rates are smaller there.

1251

1252 In figure 11, we show the NE/SW orientations of the fast-wave polarization axes of shear  
1253 waves detected by Paul et al. (2014) over most of Anatolia and the northern Aegean Sea.  
1254 These are remarkably similar to the extensional directions from GPS (e.g. fig. 7 of Le  
1255 Pichon et al. 2010) or from earthquake fault plane solutions (e.g. Floyd et al. 2010),  
1256 including the same counterclockwise rotation from eastern Anatolia to the northern  
1257 Aegean Sea noted by Paul et al. (2014). Thus the upper mantle appears to be decoupled  
1258 from the crust, flowing along the lithospheric extensional direction, toward the  
1259 easternmost Mediterranean. This direction of flow is not surprising, as the new Aegean  
1260 slab has blocked the possible outflow of the asthenosphere in the Aegean-West  
1261 Anatolian area in the last few million years. Finally, this discussion helps us to  
1262 understand why, although the westward extrusion of the Anatolia-Aegea plate was  
1263 initiated 11 Ma, the formation and westward propagation of the NAF took a few million  
1264 more years to develop, as the westward gravitational gradient was being established.

1265

## 1266 ***Conclusions***

1267

1268 The Sea of Marmara appears to be a key point in the history of the propagation of the  
1269 NAF toward the northern extremity of the Aegean subduction during the last 10 Myr.  
1270 There is no indication that a localized plate boundary existed north of the Aegean  
1271 portion of the Anatolia plate before 2 Ma. Prior to this age, the shear produced by the  
1272 motion of Anatolia with respect to Eurasia was distributed over the whole width of the  
1273 its Aegean-West Anatolian western portion. This was most probably related to the  
1274 presence there of a N/S component of extension produced by the southward migration  
1275 of the Aegean subduction. It is no coincidence that fast subduction of the oceanic Ionian

1276 lithosphere was initiated a few million years before the Anatolia westward motion.  
1277 These two processes are obviously tightly linked.

1278

1279 The beginning of the formation of a localized plate boundary occurred between 4.5 and  
1280 3.5 Ma at the location of the present Sea of Marmara by the initiation of a shear zone  
1281 comparable to the present Grecian Shear Zone in Central Greece. Thus, the first part of  
1282 the formation of the Sea of Marmara was purely extensional. The present strike-slip  
1283 system that today cuts across the whole Sea of Marmara and that is called MMF, began to  
1284 develop after 2.5 Ma. Shortly after, the plate boundary migrated westward along the  
1285 northern border of Aegea from the NAT, to the GSZ and to the Kefalonia fault. There, it  
1286 finally linked with the northern tip of the Aegean subduction zone, completing the  
1287 system of plate boundaries delimiting the Anatolia-Aegea plate. We have related the  
1288 remarkable change in the distribution of shear over Aegea from Miocene to Pliocene to  
1289 the formation of a relatively undeforming block in Pliocene that forced the shear to be  
1290 distributed over a narrow plate boundary to the north of it. We attribute the formation  
1291 of this relatively undeforming Aegean block to the northeastward progression of the  
1292 cold oceanic Ionian slab. This is because the slab cuts the overlying lithosphere from  
1293 asthenospheric sources and induces a shortening environment over it. We noted  
1294 however that another possible contribution was the lower subduction rate during the  
1295 Miocene.

1296

1297 Finally, we wish to make three remarks that may have significant implications for the  
1298 evaluation of the seismic risk in the Sea of Marmara:

1299

1300 1) The present structure of the Sea of Marmara results from the superposition of a  
1301 purely strike-slip system on top of an initial purely en-echelon extensional system. This  
1302 superposition explains the occurrence of large strike-slip earthquakes together with  
1303 significant extensional earthquakes that reactivate earlier extensional structures.

1304

1305 2) The MMF is a continuous dextral strike-slip fault through the whole basin with a  
1306 present seismic activity strikingly different from the portions of land fault broken by the  
1307 1999 Kocaeli and the 1912 Ganos earthquake. Its continuity and relative homogeneity  
1308 suggests that one cannot discard the possibility that the whole MMF will break in a  
1309 single earthquake as proposed by Le Pichon et al. (1999).

1310

1311 3) The MMF closely follows the base of the northern Marmara margin east of 28°E. As a  
1312 result there is a 4-6 km offset between the basement on both sides of the fault. Jim Rice  
1313 (personal communication to XLP, 2002) pointed out that this would induce a significant  
1314 asymmetry of elastic deformation. This asymmetry has very important implications that  
1315 have essentially been ignored up to this day.

1316

### 1317 ***Acknowledgments***

1318

1319 XLP thanks the editors of this special issue of the Canadian Journal of Earth Sciences  
1320 honouring Kevin C. Burke and John F. Dewey for their invitation to write a paper. This  
1321 presentation is one of the outcomes of fifteen years of cooperative work with many  
1322 French and Turkish colleagues. We wish to thank Michel Bouchon for communicating  
1323 important papers and theses and for discussions on the seismicity of Aegea. We thank  
1324 the reviewers Michel Bouchon, Namık Çağatay and Brian Wernicke and the editor Ali



1325 Polat for careful and very useful comments. We especially wish to thank Brian Wernicke  
1326 for many insightful suggestions.

1327

## 1328 **Annex**

1329 Moho model

1330 The model of Kende et al (in preparation) was obtained through a gravity inversion in  
1331 the Fourier domain of the measured gravity corrected from the upper crust geology. The  
1332 gravity and topography data used are satellite data [Smith et al. 1997] retrieved from  
1333 the Scripps Institution of Oceanography website. Gravity data were refined, when  
1334 possible, with the records from the Bodenseewerk KSS 31 gravimeter during the Marsite  
1335 Cruise on board the NO "Pourquoi Pas?" in October and November 2014. To avoid  
1336 superficial crustal effects, the topography was filtered with a 20 km window Gaussian  
1337 filter before being used to apply a Bouguer correction onshore. Then, the offshore  
1338 gravity was corrected from the known basin geology. The two sediment layers basin  
1339 model from Bayrakci et al. (2013) was used, completed on the southern shelf with TPAO  
1340 multichannel seismic line interpretations. The correction was made in the Fourier  
1341 domain using the Parker method [Parker 1972]. A first Moho depth variation was  
1342 computed by inverting the residual gravity anomaly and a Lower Crust/Upper Crust  
1343 boundary (LC/UC) was defined 9 km above this depth model. An iterative process was  
1344 then launched. It used the sediment basin model and the newly defined LC/UC to correct  
1345 the measured gravity with the Parker method, obtaining a new gravity residual. The  
1346 inversion of this new gravity residual led to a new Moho depth model. This process,  
1347 repeated twice, enhanced the overall model significantly as it lowered the final residual  
1348 anomaly.

1349

1350 The method developed for the study of Kende et al. (in preparation) is close to the  
1351 Parker-Oldenburg method [Oldenburg 1974] and is based on a least-square linear  
1352 inversion with preconditioning [Tarantola 2005]. This method proved to be fast and  
1353 effective for large scale 2D models. It also avoided part of the human bias associated  
1354 with forward modeling [Aitken et al. 2013]. However, because this model relies on a  
1355 simplified basin structure, the choice of the densities of the two sedimentary layers has a  
1356 strong impact on the Moho depth variation amplitude. Data well constrain the Moho  
1357 geometry only at spatial wavelengths longer than crustal thickness. To damp Moho  
1358 oscillations at shorter wavelengths, Moho deviation from the mean regional value is  
1359 preconditioned to zero and a third parameter (Moho variance scaling) entered by the  
1360 user defines the weight of this preconditioning. After defining a range of possible mean  
1361 densities for each of these parameters, the final values used for the results presented  
1362 here were those that best agreed with Bécél et al. (2009) and Karabulut et al. (2013)  
1363 Moho depth models.

1364

1365 Bécél et al. (2009) presented a Moho model based on a dense grid of Multi-channel  
1366 Marine Seismic profiles with a high penetration depth retrieved during the  
1367 SEISMARMARA Leg 1, completed with the data from on-land temporary seismometers  
1368 and Ocean Bottom Seismometers (OBSs). Their study was designed so that the profiles  
1369 crossed each other at OBS positions and had land stations in their continuity. Crossing  
1370 profiles permitted, for instance, to identify side echoes that could appear as flat interface  
1371 events on some profiles, while OBSs first arrival time of refracted waves on the  
1372 basement were used to build a basement velocity and geometry model. Finally, on land  
1373 station records of refraction on the upper mantle (Pn waves) were integrated, which  
1374 was critical for the 2D model under the Northern Marmara Trough as only 2 OBSs

1375 clearly recorded refraction on the Moho. Bécel et al. (2009) concluded that there had  
1376 been a 5 km crustal thinning below the Northern Marmara Trough and under the İmralı  
1377 Basin as the Moho height was essentially constant at a depth of 26 km. Their study  
1378 however put no constraint on the possible existence of small scale thinning variations.  
1379 Because the North-South Moho depth variation obtained was close to the data  
1380 resolution, they could not resolve conclusively the existence of possible N-S variations.

1381

1382 Karabulut et al. (2013) on the other hand published a N-S 650 km long profile of  
1383 lithospheric structures. This profile crosses the Sea of Marmara in the eastern part of the  
1384 Tekirdağ Basin. They relied on a set of 17 permanent broadband seismic stations and 23  
1385 temporary stations installed as part of the SIMBAD project to fill the gaps and create a  
1386 spacing between stations of about 15 km along the transect. After a year of recording,  
1387 they selected 60 events with a magnitude superior or equal to 5.5 and a tolerable noise  
1388 level. They then performed a depth migration of the P-to-S converted phases and  
1389 interpreted the Moho as the level of sharp increase of amplitude undulating between 25  
1390 and 32 km. Their station coverage is not tight enough at the level of the Marmara Sea to  
1391 determine the detailed Moho depth variation but Karabulut et al. (2013) showed an  
1392 uplift of 6 to 7 km centered under the sea with a width of less than 250 km. The highest  
1393 Moho under the Sea of Marmara obtained in the two studies is the same, about 25 km.

1394

## 1395 **References**

1396

1397 Aitken, A.R.A., Salmon, M.L., and Kennett, B.L.N. 2013. Australia's Moho: A test of the  
1398 usefulness of gravity modelling for the determination of Moho depth. *Tectonophysics*,  
1399 **609**: 468–479. doi:10.1016/j.tecto.2012.06.049.

1400

1401 Aksoy, M.E. 2009. Active tectonics and paleoseismology of the Ganos fault segment and  
1402 seismic characteristics of the 9 August 1012 Mürefte earthquake of the North Anatolian  
1403 fault (Western Turkey). PhD Thesis, Eurasia Institute of Earth Sciences, İstanbul  
1404 Technical University, Institute de Physique du Globe de Strasbourg, University of  
1405 Strasbourg.

1406

1407 Allen, C. 1975. Geological Criteria for Evaluating Seismicity—Address as Retiring  
1408 President of The Geological Society of America, Miami Beach, Florida, November 1974.  
1409 Geological Society of America Bulletin, **86**: 1041-1057. doi: 10.1130/0016-7606(1975).

1410

1411 Altınok, Y., and Alpar, B. 2006. Marmara Island earthquakes, of 1265 and 1935; Turkey.  
1412 Nat. Hazards Earth Syst. Sci., **6**: 999–1006.

1413

1414 Angelier, J. 1979. Néotectonique de l'Arc Egéen, Société Géologique du Nord.

1415

1416 Angelier, J., Lyberis, N., Le Pichon, X., Barrier, E., and Huchon, P. 1982. The tectonic  
1417 development of the Hellenic arc and the Sea of Crete: a synthesis. Tectonophysics, **86**:  
1418 159-196.

1419

1420 Armijo, R., Meyer, B., King, G.C.P., Rigo, A. and Papanastassiou, D. 1996. Quaternary  
1421 evolution of the Corinth Rift and its implications for the Late Cenozoic evolution of the  
1422 Aegean. Geophys. J. Int., **126**: 11–53.

1423

- 1424 Armijo, R., Meyer, B., Navarro, S., King, G., and Barka, A. 2002. Asymmetric slip  
1425 partitioning in the Sea of Marmara pull-apart: a clue to propagation processes of the  
1426 North Anatolian Fault. *Terra Nova*, **14**: 80-86.
- 1427
- 1428 Aubouin, J., Bonneau, M., Davidson, J., Leboulenger, P., Matesco, S., and Zambetakis, A.  
1429 1976. Esquisse structurale de l'arc Egéen externe: des Dinarides aux Taurides. *Bull. Soc.*  
1430 *Geol. France*, **18**: 327-336.
- 1431
- 1432 Avşar, Ü., and İşseven, T. 2009. Regional clockwise rotation of the Armutlu Peninsula,  
1433 resolved from paleomagnetic study of Eocene volcanics. *Tectonophysics*, **475**: 415-422.
- 1434
- 1435 Aydın, İ., Karat, H.İ., and Koçak, A. 2005. Curie-point depth map of Turkey. *Geophys. J.*  
1436 *Int.*, **162**: 633-640.
- 1437
- 1438 Bayrakci, G., Laigle, M., Bécel, A., Hirn, A., Taymaz, T., Yolsal-Çevikbilen, and  
1439 SEISMARMARA team 2013. 3-D sediment-basement tomography of the Northern  
1440 Marmara trough by a dense OBS network at the nodes of a grid of controlled source  
1441 profiles along the North Anatolian fault. *Geophys. J. Int.*, **194**: 1335-1357.  
1442 doi:10.1093/gji/ggt211.
- 1443
- 1444 Beaumont, C., Jamieson, R.A., Nguyen, M.H., and Medvedev, S. 2004. Crustal channel  
1445 flows: 1. Numerical models with applications to the tectonics of the Himalayan-Tibetan  
1446 orogen. *J. Geophys. Res.*, **109**: B06406. doi: 10.1029/2003JB002809.
- 1447
- 1448 Bécel, A., Laigle, M., de Voogd, B., Hirn, A., Taymaz, T., Galvé, A., Shimamura, H., Murai, Y.,

- 1449 L epine, J.C., Sapin, M., and  zalaybey, S. 2009. Moho, crustal architecture and deep  
1450 deformation under the North Marmara Trough, from the SEISMARMARA Leg 1 offshore-  
1451 onshore reflection-refraction survey. *Tectonophysics*, **467**: 1-21.
- 1452
- 1453 B cel, A., Laigle, M, de Voogd, B., Hirn, A., Taymaz, T., Yolsal-Cevikbilen, S., and  
1454 Shimamura, H. 2010. North Marmara Trough architecture of basin infill, basement and  
1455 faults, from PSDM reflection and OBS refraction seismics. *Tectonophysics*, **490**: 1-14.
- 1456
- 1457 Bijwaard, H., Spakman, W., and Engdahl, E.R. 1998. Closing the gap between regional and  
1458 global travel time tomography. *J. Geophys. Res.*, **103 (B12)**: 30055-30078.
- 1459
- 1460 Bulut, F., Bohnhoff, M., Ellsworth, W.L., Aktar, M., and Dresen, G. 2009. Microseismicity at  
1461 the North Anatolian Fault in the Sea of Marmara offshore Istanbul, NW Turkey. *J.*  
1462 *Geophys. Res.*, **114**: B09302. doi:10.1029/2008JB006244.
- 1463
- 1464  a atay, M.N., G r r, N., Alpar, B., Saat ılar, R., Akk k, R., Sakın , M., Y ce, H., Yaltırak C.,  
1465 and Kuş u.  . 1998. Geological evolution of the Gulf of Saros, NE Aegean Sea. *Geo-Marine*  
1466 *Letters*, **18**: 1-9.
- 1467
- 1468  a atay, M.N., G r r, N., Flecker, R., Sakın , M, T no lu, C., Ellam, R., Krijgsman, W.,  
1469 Vincent,S., and Dikbaş, A. 2006. Paratethyan – Mediterraenan connectivity in the Sea of  
1470 Marmara region (NW Turkey) during the Messinian. *Sedimentary Geology*, **188-189**:  
1471 171-188.
- 1472

1473 Chester, F.M., Evans, J.P., and Biegel, R.L. 1993. Internal structure and weakening  
1474 mechanism of the San Andreas fault. *J. Geophys. Res.*, **98**: 771-786.

1475

1476 Chousianitis, K., Ganas, A., and Evangelidis, C.P. 2015. Strain and rotation rates patterns  
1477 of mainland Greece from continuous GPS data and comparison between seismic and  
1478 geodetic moment release. *J. Geophys. Res. (Solid Earth)*, **120**: 3909-3931.  
1479 doi:10.1002/2014JB011762.

1480

1481 Cocard, M., Kahle, H.-G., Peter, Y., Geiger, A., Veis, G., Felekis, S., Paradissis, D., and  
1482 Billiris, H. 1999. New constraints on the rapid crustal motion of the Aegean region:  
1483 Recent results inferred from GPS measurements (1993–1998) across the West Hellenic  
1484 arc, Greece. *Earth Planet. Sci. Lett.*, **172**: 39–47.

1485

1486 Drooger, C.W., and Meulenkaamp, J.E. 1973. Stratigraphic contribution to geodynamics in  
1487 the Mediterranean Area: Crete as a case history. *Bull. Soc. Geol. Greece*, **10**: 193-200.

1488

1489 Durand, V., Bouchon, M., Floyd, M.A., Theodulidis, N., Marsan, D., Karabulut, H., and  
1490 Schmittbuhl, J. 2014. Observation of the spread of slow deformation in Greece following  
1491 the breakup of the slab. *Geophys. Res. Lett.*, **41**: 7129–7134.  
1492 doi:10.1002/2014GL061408.

1493

1494 Faccenna C, Bellier O, Martinod J, Piromallo C, and Regard V. 2006. Slab detachment  
1495 beneath eastern Anatolia: a possible cause for the formation of the North Anatolian  
1496 Fault. *Earth Planet. Sci. Lett.*, **242**: 85–79.

1497

- 1498 Flesch, L.M., Haines, A.J., and Holt, W.E. 2005, Constraining the extent of crust-mantle  
1499 coupling in central Asia using GPS, geologic, and shear-wave splitting data, *Earth Planet.*  
1500 *Sci. Lett.*, **238**: 248-268.
- 1501
- 1502 Floyd, M.A., Billiris, H., Paradissis, D., Veis, G., Avallone, A., Briole, P., McClusky, S.,  
1503 Nocquet, J.-M., Palamartchouk, K., Parsons, B., and England, P.C. 2010. A new velocity  
1504 field for Greece: Implications for the kinematics and dynamics of the Aegean. *J. Geophys.*  
1505 *Res.*, **115**: B10403. doi:10.1029/2009JB007040.
- 1506
- 1507 Flotté, N. 2003. Caractérisation Structurale et Cinématique d'un Rift sur Détachement:  
1508 Le Rift de Corinthe-Patras, Grèce. Thèse de Doctorat, Orsay: Univ. Paris-Sud.
- 1509
- 1510 Friedrich, A.M., Lee, J., Wernicke, B.P. and Sieh, K. 2004. Geologic context of geodetic data  
1511 across a Basin and Range normal fault, Crescent Valley, Nevada. *Tectonics*, **23**: TC2015.  
1512 doi:10.1029/2003TC001528.
- 1513
- 1514 Gasperini, L., Polonia, A., Çağatay, M.N., Bortoluzzi, G., and Ferrante, V. 2011. Geological  
1515 slip rate along the North Anatolian Fault in the Marmara region. *Tectonics*, **30**: TC6001.  
1516 doi:10.1029/2011TC002906.
- 1517
- 1518 General Directorate of Mineral Research and Exploration, 2002. 1/500 000 Geological  
1519 Map of Turkey
- 1520
- 1521 Goldsworthy, M., Jackson, J., and Haines, J. 2002. The continuity of active fault systems in  
1522 Greece. *Geophys. J. Int.*, **148(3)**: 596–618. doi:10.1046/j.1365-246X.2002.01609.x.



1523

1524 Görgün, E., and Görgün, B. 2015. Seismicity of the 24 May 2014 Mw 7.0 Aegean Sea  
1525 earthquake sequence along the North Aegean Trough. *Journal of Asian Earth Sciences*,  
1526 doi:10.1016/j.jseaes.2015.06.018.

1527

1528 Görür, N., Çağatay, M.N., Sakıncı, M., Sümengen, M., Şentürk, K., Yaltrak, C., and  
1529 Tchaplalyga, A. 1997. Origin of the Sea of Marmara deduced from Neogene to Quaternary  
1530 paleogeographic exposition of its framework. *Intern. Geology Rev.*, **39**: 342-352.

1531

1532 Grall, C., Henry, P., Tezcan, D., Mercier de Lepinay, B., Bécel, A., Geli, L., Rudkiewicz, J.-L.,  
1533 Zitter, T., and Harmegnies, F. 2012. Heat flow in the Sea of Marmara Central Basin:  
1534 Possible implications for the tectonic evolution of the North Anatolian fault. *Geology*,  
1535 **40(1)**: 3–6. doi:10.1130/G32192.1.

1536

1537 Grall, C., Henry, P., Thomas, Y., Westbrook, G.K., Çağatay, M.N., Marsset, B., Saritas, H.,  
1538 Cifci, G., and Géli, L. 2013. Slip rate estimation along the western segment of the Main  
1539 Marmara Fault over the last 405-490 ka by correlating Mass Transport Deposits.  
1540 *Tectonics*, **32(6)**: 1587–1601.

1541

1542 Gudmundsson, O., and Sambridge, M. 1998. A regionalized upper mantle (RUM) seismic  
1543 model. *J. Geophys. Res.*, **103(B4)**: 7121–7136.

1544

1545 Holt, W.E. 2000. Correlated crust and mantle strain fields in Tibet. *Geology*, **28**: 67-70.

1546

1547 Hubert-Ferrari, A., Armijo, R., King, G., Meyer, B., and Barka, A. 2002. Morphology,

1548 displacement, and slip rates along the North Anatolian fault, Turkey. *J. Geophys. Res.*,  
1549 **107(B10)**: doi:10.1029/2001JB000393.

1550

1551 Jackson, J., and McKenzie. D. 1989. Relation between seismicity and paleomagnetic  
1552 rotation in zones of distributed continental deformation. *In* *Paleomagnetic Rotations*  
1553 *and Continental Deformation*. Edited by C. Kissel and C. Laj. Kluwer Academic  
1554 Publishers, The Hague. pp. 33-49.

1555

1556 Jolivet, L., and Brun, J.P. 2010. Cenozoic geodynamic evolution of the Aegean. *Int. J. Earth*  
1557 *Sci. (Geol. Rundsch.)*, **99**: 109–138. doi:10.1007/s00531-008-0366-4.

1558

1559 Jolivet, L., Labrousse, L., Agard, P., Lacombe, O., Bailly, V., Lecomte, E., Mouthereau, F.,  
1560 and Mehl, C. 2010. Rifting and shallow-dipping detachments, clues from the Corinth Rift  
1561 and the Aegean. *Tectonophysics*, **483**: 287–304.

1562

1563 Karabulut, H., Bouin, M.P., Bouchon, M., Dietrich, M., Cornou, C., and Aktar, M. 2002. The  
1564 Seismicity in the Eastern Marmara Sea after the 17 August 1999 İzmit Earthquake.  
1565 *Bulletin of the Seismological Society of America*, **92(1)**: 387-393.

1566

1567 Karabulut, H., Roumelioti, Z., Benetatos, C., Köméc-Mutlu, A., Özalaybey, S., Aktar, M., and  
1568 Kiratzi, A. 2006. A source study of the 6 July 2003 ( $M_w$  5.7) earthquake sequence in the  
1569 Gulf of Saros (Northern Aegean Sea): Seismological evidence for the western  
1570 continuation of the Ganos fault. *Tectonophysics*, **412**: 195-216.

1571

1572 Karabulut, H., Schmittbuhl, J., Özalaybey, S., Lengliné, O., Köméc-Mutlu, A., Durand, V.,

- 1573 Bouchon, M., Daniel, G., and Bouin, M.P. 2011. Evolution of the seismicity in the eastern  
1574 Marmara Sea a decade before and after the 17 August 1999 Izmit earthquake.  
1575 *Tectonophysics*, **510**: 17-27.
- 1576
- 1577 Karabulut, H., Paul, A., Ergün, T.A., Hatzfeld, D., Childs, D.M., and Aktar, M. 2013. Long-  
1578 wavelength undulations of the seismic Moho beneath the strongly stretched Western  
1579 Anatolia. *Geophys. J. Int.*, **194(1)**: 450-464. doi: 10.1093/gji/ggt100.
- 1580
- 1581 Karabulut, H., Paul, A., Cambaz, D., Kömeç Mutlu, A., Aksarı, D., and Afacan Ergün, T.  
1582 2015. The Images of Anatolia. EGU General Assembly, 12-17 April, 2015, Vienna,  
1583 Austria. id.8921.
- 1584
- 1585 Kastens, K.A. 1991. Rate of outward growth of the Mediterranean Ridge accretionary  
1586 complex. *Tectonophysics*, **199**: 25-50.
- 1587
- 1588 Kende, J., Henry, P., Bayrakci, G. et al. 2015. Moho depth and crustal thinning in the  
1589 Marmara Sea region from gravity data inversion. In preparation.
- 1590
- 1591 Kissel, C., Laj, C., Poisson, A. and Görür, N. 2003. Paleomagnetic reconstruction of the  
1592 Cenozoic evolution of the eastern Mediterranean. *Tectonophysics*, **362**: 199-217.
- 1593
- 1594 Kozacı, Ö., Dolan, J.F., and Finkel, R.C. 2009. A late Holocene slip rate for the central  
1595 North Anatolian fault, at Tahtaköprü, Turkey, from cosmogenic <sup>10</sup>Be geochronology:  
1596 Implications for fault loading and strain release rates. *J. Geophys. Res.*, **114**: B01405.  
1597 doi:10.1029/2008JB005760.

1598

1599 Kurt, H., Demirbağ, E., and Kuşçu, İ. 2000. Active submarine tectonism and formation of  
1600 the Gulf of Saros, Northeast Aegean Sea, inferred from multi-channel seismic reflection  
1601 data. *Marine Geology*, **165**: 13–26.

1602

1603 Kurt, H., Sorlien, C.C., Seeber, L., Steckler, M.S., Shillington, D.J., Cifci, G., Cormier, M.H.,  
1604 Dessa, J.X., Atgin, O., Dondurur, D., Demirbag, E., Okay, S., Imren, C., Gurcay, S., and  
1605 Carton, H. 2013. Steady late quaternary slip rate on the Cinarcik section of the North  
1606 Anatolian fault near Istanbul, Turkey. *Geophys. Res. Lett.*, **40**: 4555–4559.  
1607 doi:10.1002/grl.50882.

1608

1609 Laigle, M., Bécel, A., de Voogd, B., Hirn, A., Taymaz, T., Ozalaybey, S., and members of  
1610 SEISMARMARA Leg1 Team 2008. A first deep seismic survey in the Sea of Marmara:  
1611 Deep basins and whole crust architecture and evolution. *Earth Planet. Sci. Lett.*, **270**:  
1612 168–179.

1613

1614 Le Pichon, X., and Angelier, J. 1979. The Hellenic arc and trench system: a key to the  
1615 neotectonic evolution of the Eastern Mediterranean area. *Tectonophysics*, **60**: 1-42.

1616

1617 Le Pichon, X., and Angelier, J. 1981. The Aegean Sea. *Phil. Trans. R. Soc. London*, **A300**:  
1618 357-372.

1619

1620 Le Pichon, X. 1982. Land-locked oceanic basins and continental collision: the eastern  
1621 Mediterranean as a case example. In *Mountain Building Processes*. Edited by K.J. Hsü.  
1622 Academic Press, London. pp. 201–211.

1623

1624 Le Pichon, X., Fournier, M. and Jolivet, L. 1992. Kinematics, topography, shortening, and  
1625 extrusion in the India-Eurasia collision. *Tectonics*, **11(6)**: 1085-1098.

1626

1627 Le Pichon X., Chamot-Rooke N., Huchon P., and Luxey P. 1993. Implication des nouvelles  
1628 mesures de géodésie spatiale en Grèce et Turquie sur l'extrusion latérale de l'Anatolie et  
1629 de l'Egée. *C. R. Acad. Sci. Paris II*, **316**: 983-990.

1630

1631 Le Pichon, X., Chamot-Rooke, N., Lallemand, S., Noomen, R., and Veis, G. 1995. Geodetic  
1632 determination of the kinematics of central Greece with respect to Europe: implications  
1633 for eastern Mediterranean tectonics. *J. Geophys. Res.*, **100**: 12675-12690.

1634

1635 Le Pichon, X., Taymaz, T., and Şengör, A.M.C. 1999. The Marmara fault and the future  
1636 Istanbul earthquake. In ITU-IAHS International Conference on the Kocaeli earthquake 17  
1637 August 1999. Edited by M. Karaca and D.N. Ural. Istanbul Technical University, Turkey.  
1638 pp. 41-54.

1639

1640 Le Pichon, X., Şengör, A.M.C., Demirbağ, E., Rangin, C., İmren, C., Armijo, R., Görür, N.,  
1641 Çağatay, N., Mercier de Lepinay, B., Meyer, B., Saatçılar, R., and Tok, B. 2001. The active  
1642 main Marmara fault. *Earth Planet. Sci. Lett.*, **192**: 595-616.

1643

1644 Le Pichon, X., Lallemand, S.J., Chamot-Rooke, N., Lemeur, D., and Pascal, G. 2002. The  
1645 Mediterranean Ridge backstop and the Hellenic nappes. *Marine Geology*, **186**: 111-125.

1646

- 1647 Le Pichon, X., Chamot-Rooke, N., Rangin, C., and Şengör, A.M.C. 2003. The North  
1648 Anatolian Fault in the Sea of Marmara. *J. Geophys. Res.*, **108(B4)**: 2179.  
1649 doi:10.1029/2002JB001862.
- 1650
- 1651 Le Pichon, X., and Kreemer, C. 2010. The miocene-to-present kinematic evolution of the  
1652 Eastern Mediterranean and Middle East and its implications for dynamics. *Ann Rev*  
1653 *Earth Planet. Sci.*, **38**: 323–351.
- 1654
- 1655 Le Pichon, X., İmren, C., Rangin, C., Şengör, A.M.C. and Siyako, M. 2014. The South  
1656 Marmara Fault. *Int J Earth Sci (Geol Rundsch)*, **103**: 219–231. doi 10.1007/s00531-013-  
1657 0950-0.
- 1658
- 1659 Lister, C.S., Banga, G., and Feenstra, A. 1984. Metamorphic core complexes of Cordilleran  
1660 type in the Cyclades, Aegean Sea, Greece. *Geology*, **12**: 221-225.
- 1661
- 1662 Martinod, J., Hatzfeld, D., Brun, J.P., Davy, P., and Gautier, P. 2000. Continental collision,  
1663 gravity spreading, and kinematics of Aegea and Anatolia. *Tectonics*, **19(2)**: 290–299.
- 1664
- 1665 Mascle, J., and Martin, L. 1990. Shallow structure and recent evolution of the Aegean Sea:  
1666 A synthesis based on continuous reflection profiles. *Marine Geology*, **94(4)**: 271-299.
- 1667
- 1668 McClusky, S., Balassanian, S., Barka, A., Demir, C., Ergintav, S., Georgiev, I. Gurkan, O.,  
1669 Hamburger, M., Hurst, K., Kahle, H., Kastens, K., Kekelidze, G., King, R., Kotzev, V., Lenk,  
1670 O., Mahmoud, S., Mishin, A., Nadariya, M., Ouzounis, A., Paradissis, D., Peter, Y., Prilepin,  
1671 M., Reilinger, R., Sanli, I., Seeger, H., Tealeb, A., Toksöz, M.N., and Veis, G. 2000. Global

- 1672 positioning system constraints on plate kinematics and dynamics in the eastern  
1673 Mediterranean and Caucasus. *J. Geophys. Res.*, **105(B3)**: 5695–5719.
- 1674
- 1675 McClusky, S., Reilinger, R., Mahmoud, S., Sari, D.B., and Tealeb, A. 2003. GPS constraints  
1676 on Africa (Nubia) and Arabia plate motions. *Geophys. J. Int.*, **155**: 126–138.
- 1677
- 1678 McKenzie, D.P. 1970. Plate tectonics of the Mediterranean region. *Nature*, **226(5242)**:  
1679 239–243.
- 1680
- 1681 McKenzie, D.P. 1972. Active tectonics of the Mediterranean region. *Geophys. J. R. Astron.*  
1682 *Soc.*, **30**: 109–185.
- 1683
- 1684 McKenzie, D., and Jackson, J. 1983. The relationship between strain rates, crustal  
1685 thickening, palaeomagnetism, finite strain and fault movements within a deforming  
1686 zone. *Earth Planet. Sci. Lett.*, **65(1)**: 182-202.
- 1687
- 1688 McKenzie, D., and Jackson, J. 1986. A block model of distributed deformation by faulting.  
1689 *J. Geol. Soc. London*, **143(2)**: 349-353.
- 1690
- 1691 McKenzie, D., and Jackson, J. 1989. The kinematics and dynamics of distributed  
1692 deformation. *In* *Paleomagnetic Rotations and Continental Deformation*. Edited by C.  
1693 Kissel and C. Laj. Kluwer Academic Publishers, The Hague. pp. 33-49.
- 1694
- 1695 McKenzie, D., and Jackson, J. 2002. Conditions for flow in the continental crust.  
1696 *Tectonics*, **21(6)**: doi:1010.1029/2002TC001394.

1697

1698 McKenzie, D., Jackson, J., and Priestley, K. 2005. Thermal structure of oceanic and  
1699 continental lithosphere. *Earth Planet. Sci. Lett.*, **233**: 337–349.

1700

1701 Meade, B.J., Hager, B.H., McClusky, S.C., Reilinger, R.E., Ergintav, S., Lenk, O., Barka, A., and  
1702 Özener, H. 2002. Estimates of seismic potential in the Marmara Sea region from block  
1703 models of secular deformation constrained by global positioning system measurements.  
1704 *Bull. Seismol. Soc. Am.*, **92(1)**: 208–215.

1705

1706 Meghraoui, M., Aksoy, M.E., Aksyüz, H.S., Ferry, M., Dikbaş, A., and Altunel, E. 2012.  
1707 Paleoseismology of the North Anatolian Fault at Güzelköy (Ganos segment, Turkey): Size  
1708 and recurrence time of earthquake ruptures west of the Sea of Marmara. *Geochem.  
1709 Geophys. Geosyst.*, **13(4)**: Q04005. doi:10.1029/2011GC003960.

1710

1711 Melinte-Dobrinescu, M.C., Suc J-P., Clauzon, G., Popescu, S-M., Armijo, R., Meyer B.,  
1712 Biltekin, D., Çağatay, M.N., Uçarkuş, G, Jouannic, G, Fauquette, S, and Çakir, Z. 2009. The  
1713 Messinian Salinity Crisis in the Dardanelles region: Chronostratigraphic constraints.  
1714 *Paleogeography, Paleocyanography, Paleoclimatology*, **278**: 24–39.

1715

1716 Müller, M.D., Geiger, A., Kahle, H.G., Veis, G., Billiris, H., Paradissis, D., and Felekis, S. 2013.  
1717 Velocity and deformation fields in the North Aegean domain, Greece, and implications  
1718 for fault kinematics, derived from GPS data 1993-2009. *Tectonophysics*, **597-598**: 34-  
1719 49.

1720



- 1721 Nielsen, C. 2003. Etude des zones de subduction en convergence hyper-oblique: ride  
1722 méditerranéenne, marge indo-birmane. Thèse de doctorat, Université Paris XI, Orsay.  
1723
- 1724 Oldenburg, D.W. 1974. The Inversion and interpretation of gravity anomalies.  
1725 *Geophysics*, **39(4)**: 526–536. doi:10.1190/1.1440444.  
1726
- 1727 Oncken, O., Chong, G., Franz, G., Giese, P., Götze, H.-J., Ramos, V.A., Strecker, M.R., and  
1728 Wigger, P. 2006. An Andes: Active Subduction Orogeny (Frontiers in the Earth Sciences  
1729 Series). Springer, Berlin.  
1730
- 1731 Örgülü, G. 2011. Seismicity and source parameters for small-scale earthquakes along the  
1732 splays of the North Anatolian Fault (NAF) in the Marmara Sea. *Geophys. J. Int.*, **184(1)**:  
1733 385–404.  
1734
- 1735 Parker, R.L. 1972. The Rapid Calculation of Potential Anomalies. *Geophys. J. R. astr. Soc.*,  
1736 **31(4)**: 447–455. doi:10.1111/j.1365-246X.1973.tb06513.x.  
1737
- 1738 Paul, A., Karabulut, H., Kömec-Mutlu, A., and Salaün, G. 2014. A comprehensive and  
1739 densely sampled map of shear-wave azimuthal anisotropy in the Aegean-Anatolia  
1740 region. *Earth Planet. Sci. Lett.*, **389**: 14-22.  
1741
- 1742 Pearce, F.D. 2015. Seismic imaging of the western Hellenic subduction zone: The  
1743 relationship between slab composition, retreat rate, and overriding lithosphere genesis.  
1744 PhD thesis, Department of Earth, Atmospheric, and Planetary Sciences, Massachusetts  
1745 Institute of Technology, Cambridge, MA, USA.

1746

1747 Pérouse, E., Chamot-Rooke, N., Rabaute, A., Briole, P., Jouanne, F., Georgiev, I., and  
1748 Dimitrov, D. 2012. Bridging onshore and offshore present-day kinematics of central and  
1749 eastern Mediterranean: Implications for crustal dynamics and mantle flow. *Geochem.*  
1750 *Geophys. Geosyst.*, **13(9)**: Q09013. doi:10.1029/2012GC004289.

1751

1752 Piromallo, C., and Morelli, A. 2003. P wave tomography of the mantle under the Alpine-  
1753 Mediterranean area. *J. Geophys. Res.*, **108(B2)**: 2065. doi:10.1029/2002JB001757.

1754

1755 Provost, A.S., Chéry, J., and Hassani, R. 2003. 3-D mechanical modeling of the GPS  
1756 velocity field along the North Anatolian Fault. *Earth Planet. Sci. Lett.*, **209**: 361–377.

1757

1758 Rangin, C., Le Pichon, X., Demirbag, E. and Imren, C. 2004. Strain localization in the Sea of  
1759 Marmara: propagation of the North Anatolian Fault in a now inactive pull-apart.  
1760 *Tectonics*, **23**: TC2014. doi:10.1029/2002TC001437.

1761

1762 Reilinger, R.E., McClusky, S.C., Oral, M.B., King, R.W., Toksoz, M.N., Barka, A.A., Kinik, I.,  
1763 Lenk, O. and Sanli, I. 1997. Global positioning system measurements of present-day  
1764 crustal movements in the Arabia-Africa-Eurasia plate collision zone. *J. Geophys. Res.*,  
1765 **102(B5)**: 9983–9999.

1766

1767 Reilinger, R., McClusky, S., Vernant, P., Lawrence, S., Ergintav, S., Cakmak, R., Ozener, H.,  
1768 Kadirov, F., Guliev, I., Stepanyan, R., Nadariya, M., Habubia, G., Mahmoud, S., Sakr, K.,  
1769 ArRajehi, A., Paradissis, D., Al-Aydrus, A., Prilepin, M., Guseva, T., Evren, E., Dmitrotsa, A.,  
1770 Filikov, S.V., Gomez, F., Al-Ghazzi, R., and Karam, G. 2006. GPS constraints on continental

1771 deformation in the Africa-Arabia-Eurasia continental collision zone and implications for  
1772 the dynamics of plate interactions. *J. Geophys. Res.*, **111(B5)**:  
1773 doi:10.1029/2005JB004051.

1774

1775 Rigo, A., Lyon-Caen, H., Armijo, R., Deschamps, A., Hatzfeld, D., Makropoulos, K.,  
1776 Papadimitriou, P., and Kassaras, I. 1996. A microseismic study in the western part of the  
1777 Gulf of Corinth (Greece): implications for large-scale normal faulting mechanisms.  
1778 *Geophys. J. Int.*, **126(3)**: 663-688.

1779

1780 Royden, L.H., and Husson, L. 2006. Trench motion, slab geometry and viscous stresses in  
1781 subduction systems. *Geophys. J. Int.*, **167(2)**: 881-905. doi:10.1111/j.1365-  
1782 246X.2006.03079.x.

1783

1784 Royden, L.H., and Papanikolaou, D.J. 2011. Slab segmentation and late Cenozoic  
1785 disruption of the Hellenic arc. *Geochem. Geophys. Geosyst.*, **12(3)**: Q03010.  
1786 doi:10.1029/2010GC003280.

1787

1788 Royden, L.H., Burchfiel, B.C. and van der Hilst, R.D. 2008. The geological evolution of the  
1789 Tibetan Plateau. *Science*, **321**: 1054-1058.

1790

1791 Sakıncı, M., Yaltrak, C., and Oktay, F.Y. 1999. Palaeogeographical evolution of the Thrace  
1792 Neogene Basin and the Tethys-Paratethys relations at northwestern Turkey (Thrace).  
1793 *Palaeogeography, Palaeoclimatology, Palaeoecology*, **153**: 17-40.

1794

1795 Salaün, G., Pedersen, H.A., Paul, A., Farra, V., Karabulut, H., Hatzfeld, D., Papazachos, C.,

1796 Childs, D.M., Pequegnat, C., and SIMBAAD Team 2012. High resolution surface wave  
1797 tomography beneath the Aegean-Anatolia region: constraints on upper-mantle  
1798 structure. *Geophys. J. Int.*, **190(1)**: 406–420. doi:10.1111/j.1365-246X.2012.05483.x.

1799

1800 Seeber, L., Emre, O., Cormier, M.-H., Sorlien, C. C., McHugh, C., Polonia, A., Ozer, N.,  
1801 Cagatay, N., and the team of the 2000 R/V Urania Cruise in the Marmara Sea 2004. Uplift  
1802 and subsidence from oblique slip: the Ganos–Marmara bend of the North Anatolian  
1803 Transform, western Turkey. *Tectonophysics*, **391(1-4)**: 239–258.  
1804 doi:10.1016/j.tecto.2004.07.015.

1805

1806 Seeber, L., Cormier, M.H., McHugh, C., Emre, O., Polonia, A., and Sorlien, C. 2006. Rapid  
1807 subsidence and sedimentation from oblique slip near a bend on the North Anatolian  
1808 transform fault in the Marmara Sea, Turkey. *Geology*, **34(11)**: 933-936.

1809

1810 Şengör, A.M.C. 1979. The North Anatolian Transform Fault: its age, offset and tectonic  
1811 significance. *Jour. Geol. Soc. London*, **136**: 269-282.

1812

1813 Şengör, A.M.C. 1982. Ege'nin neotektonik evrimini yöneten etkenler [Factors controlling  
1814 the neotectonics of the Aegean] In *Batı Anadolu'nun Genç Tektoniği ve Volkanizması*.  
1815 Edited by O. Erol and V. Oygür. Türkiye Jeoloji Kurumu, Ankara, pp. 59-71.

1816

1817 Şengör, A.M.C., Burke, K., and Dewey, J.F. 1982. Tectonics of the North Anatolian  
1818 transform fault. *In Multidisciplinary Approach to Earthquake Prediction*. Edited by A.M.  
1819 Işıkara and A. Vogel. Friedr. Vieweg Sohn, Braunschweig/Wiesbaden, pp. 3-22.

1820

1821 Şengör, A.M.C., Özeren, S., Genç, T., and Zor, E. 2003. East Anatolian high plateau as  
1822 mantle-supported, north-south shortened domal structure? *Geophys. Res. Lett.*, **30(24)**:  
1823 doi:10.1029/2003GL017858.

1824

1825 Şengör, A.M.C., Tüysüz, O., İmren, C., Sakıncı, M., Eyidoğan, H., Görür, N., Le Pichon, X., and  
1826 Rangin, C. 2005. The North Anatolian Fault: A new look. *Annu. Rev. Earth Planet. Sci.*, **33**:  
1827 37–112.

1828

1829 Şengör, A.M.C., Grall, C., İmren, C., Le Pichon, X., Görür, N., Henry, P., Karabulut, H., and  
1830 Siyako, M. 2014. The geometry of the North Anatolian transform fault in the Sea of  
1831 Marmara and its temporal evolution: implications for the development of  
1832 intracontinental transform faults. *Can. J. Earth Sci.*, **51**: 222–242. doi:10.1139/cjes-2013-  
1833 0160.

1834

1835 Şengör, A.M.C., and Zabcı, C. in press. The North Anatolian Fault and the North Anatolian  
1836 Shear Zone. In *Landscapes of Turkey*. Edited by C. Kuzucuoğlu and A. Ciner. Springer,  
1837 Berlin.

1838

1839 Shaw, B., and Jackson, J. 2010. Earthquake mechanisms and active tectonics of the  
1840 Hellenic subduction zone. *Geophys. J. Int.*, **181(2)**: 966–984. Doi:10.1111/j.1365-  
1841 246X.2010.04551.x.

1842

1843 Smith, W.H.F., and Sandwell, D.T. 1997. Global Sea Floor Topography from Satellite  
1844 Altimetry and Ship Depth Soundings. *Science*, **277**: 1956–1962.  
1845 doi:10.1126/science.277.5334.1956.

1846

1847 Sonder, L.J., and England, P.C. 1989. Effects of a temperature-dependent rheology on  
1848 large-scale continental extension. *J. Geophys. Res.*, **94(B6)**: 7603–7619.

1849

1850 Sorel, D. 2000. A Pleistocene and still-active detachment fault and the origin of the  
1851 Corinth-Patras rift, Greece. *Geology*, **28(1)**: 83–86.

1852

1853 Sorlien, C.C., Akhun, S.D., Seeber, L., Steckler, M.S., Shillington, D.J., Kurt, H., Çifçi, G.,  
1854 Timur Poyraz, D., Gürçay, S., Dondurur, D., İmren, C., Perinçek, E., Okay, S., Küçük, H.M.,  
1855 and Diebold, J.B. 2012. Uniform basin growth over the last 500ka, North Anatolian Fault,  
1856 Marmara Sea, Turkey. *Tectonophysics*, **518-521**: 1–16. doi:10.1016/j.tecto.2011.10.006.

1857

1858 Spakman, W., van der Lee, S., and van der Hilst, R. 1993. Travel time tomography of the  
1859 European-Mediterranean mantle down to 1400 km. *Phys. Earth Planet. Int.*, **79(1-2)**: 3-  
1860 74.

1861

1862 Spencer, J.E. 1984. The role of tectonic denudation in the warping and uplift of low-angle  
1863 normal faults. *Geology*, **12**: 95-98.

1864

1865 Steckler, M.S., and ten Brink, U.S. 1986. Lithospheric strength variations as a control on  
1866 new plate boundaries: examples from the northern Red Sea region. *Earth Planet. Sci.*  
1867 *Lett.*, **79(1-2)**: 120-132.

1868

1869 Suckale, J., Rondenay, S., Sachpazi, M., Charalampakis, M., Hosa, A., and Royden, L.H.  
1870 2009. High-resolution seismic imaging of the western Hellenic subduction zone using

- 1871 teleseismic scattered waves. *Geophys. J. Int.*, **178(2)**: 775–791. doi:10.1111/j.1365-  
1872 246X.2009.04170.x.
- 1873
- 1874 Sümengen, M., Terlemez, İ., Şentürk K, Karaköse, C., Erkan, E., Ünay E., Gürbüz, M. and  
1875 Atalay, Z. 1987. Stratigraphy, sedimentology, and tectonics of the Tertiary sequences in  
1876 Gelibolu Peninsula and southwestern Thrace (in Turkish). Mineral Research and  
1877 Exploration of Turkey. Tech. Rep. 8128.
- 1878
- 1879 Tarantola, A. 2005. Inverse Problem Theory and Methods for Model Parameter  
1880 Estimation. Society for Industrial and Applied Mathematics.
- 1881
- 1882 Tiberi, C., Diament, M., Lyon-Caen, H., and King, T. 2001. Moho topography beneath the  
1883 Corinth Rift area (Greece) from inversion of gravity data. *Geophys. J. Int.*, **145(3)**: 797–  
1884 808.
- 1885
- 1886 Tirel, C., Gueydan, F., Tiberi, C., and Brun, J.P. 2004. Aegean crustal thickness inferred  
1887 from gravity inversion. *Earth and Planetary Science Letters*, **228**: 267-280.
- 1888
- 1889 Tirel, C., Brun, J.P., Burov, E., Wortel, M.J.R., and Lebedev, S. 2013. A plate tectonics  
1890 oddity: Caterpillar-walk exhumation of subducted continental crust. *Geology*, **41(5)**:  
1891 555-558.
- 1892
- 1893 Tüysüz, O., Barka, A., and Yiğitbaş, E. 1998. Geology of the Saros graben and its  
1894 implications for the evolution of the North Anatolian fault in the Ganos–Saros region,  
1895 northwestern Turkey. *Tectonophysics*, **293(1-2)**: 105–126.

1896

1897 Truffert, C., Chamot-Rooke, N., Lallemand, S., de Voogd, B., Huchon, P., and Le Pichon, X.  
1898 1993. The crust of the Western Mediterranean Ridge from deep seismic data and gravity  
1899 Modelling. *Geophys. J. Int.*, **114(2)**: 360-372.

1900

1901 Ustaömer, T., Gökaşan, E., Tur, H., Görüm, T., Batuk, F.G., Kalafat, D., Alp, H., Ecevitoğlu,  
1902 B., and Birkan, H. 2008. Faulting, mass-wasting and deposition in an active dextral shear  
1903 zone, the Gulf of Saros and the NE Aegean Sea, NW Turkey. *Geo-Mar. Lett.*, **28(3)**: 171-  
1904 193.

1905

1906 Van Hinsbergen, D.J.J., Langereis, C.G., and Meulenkamp, J.E. 2005. Revision of the  
1907 timing, magnitude and distribution of Neogene rotations in the western Aegean  
1908 region. *Tectonophysics*, **396(1-2)**: 1-34. doi:10.1016/j.tecto.2004.10.001.

1909

1910 Van Hinsbergen, D.J.J., Dekkers, M.J., Bozkurt, E. and Koopman, M. 2010. Exhumation  
1911 with a twist: Paleomagnetic constraints on the evolution of the Menderes metamorphic  
1912 core complex, western Turkey. *Tectonics*. **29(3)**: TC3009. doi:10.1029/2009TC002596.

1913

1914 Vassilikis, E., Royden, L., and Papanikolaou, D. 2011. Kinematic links between  
1915 subduction along the Hellenic trench and extension in the Gulf of Corinth, Greece: A  
1916 multidisciplinary analysis. *Earth and Planetary Science Letters*, **303(1-2)**: 108-120.

1917

1918 Vernant, P., Reilinger, R., and McClusky, S. 2014. Geodetic evidence for low coupling on  
1919 the Hellenic subduction plate interface. *Earth Planet. Sci. Lett.*, **385**: 122-129.

1920



1921 Wernicke, B., Walker, J.D. and Baufait, M.S. 1985. Structural discordance between  
1922 Neogene detachments and frontal Sevier thrusts, Central Mormon mountains, southern  
1923 Nevada. *Tectonics*, **4(2)**: 213-246.

1924

1925 Wernicke, B., Davis, J.L., Niemi, N.A., Luffi, P., and Bisnath, S. 2008. Active  
1926 megadetachment beneath the western United States. *J. Geophys. Res.*, **113**: B11409.  
1927 doi:10.1029/2007JB005375.

Draft

1928

1929 **Captions**

1930

1931 *Figure 1*

1932 Tectonic map of Aegea-Western Anatolia. Violet indicate shortening structures Yellow,  
1933 normal faults Green, left-slip faults White, North-Anatolian dextral fault family including  
1934 the normal faults of the Grecian Shear Zone (Şengör 1979). All faults are Quaternary,  
1935 because they cut Quaternary deposits established by sequence correlations in the Sea of  
1936 Marmara. Following Clarence Allen's rule (Allen 1975), we assume all are active or  
1937 potentially so. The light colored presently undeforming Aegean block revealed by  
1938 geodesy is limited by dashed lines. The dashed red contours of the Aegean slab are after  
1939 Gudmundsson and Sambridge (1988). The two yellowish shear zones that limit it, the  
1940 GSZ and NAT to the north with clockwise rotation and the WASZ to the east with  
1941 counterclockwise rotation, absorb about 20-25 mm/yr of shear, dextral for the northern  
1942 zone and sinistral for the eastern one. The figure is modified from Şengör and Zabcı (in  
1943 press).

1944

1945 *Figure 2*

1946 Proposed tectonic map of Aegea-Western Anatolia about 4 Ma. White line, the westward  
1947 propagating North-Anatolian dextral system has just reached the area of the present Sea  
1948 of Marmara that is occupied by a system of clockwise rotating normal-fault bounded  
1949 blocks similar to the GSZ, with extensional decollements in front the tip of the NAF.  
1950 Modified from Şengör and Zabcı (in press)

1951

1952 *Figure 2.5*

1953 Index map of geographic and geologic features within the Sea of Marmara area  
1954 discussed in the text.

1955

1956 *Figure 3a*

1957 Map of the southern shelf anticlinal system. Faults on the shelf after Le Pichon et al.  
1958 (2014). Contours every 100 m. (light lines) and 500 m. (dark lines) are estimates of  
1959 amount of eroded material based on the seismic profiles. See Le Pichon et al. (2014) for  
1960 network of seismic profiles used. The 3.5 Ma South Marmara Fault (SMF) is shown in  
1961 red. Possible x-shears related to the clockwise rotation of the blocks between 4 and 3.5  
1962 Ma are shown as dotted lines, in purple. Red barbed lines are direction of propagation of  
1963 clastics. Contours between the sea floor and 13 km depth of detachments north of the  
1964 Marmara anticline after Bécel et al. (2009). Black lines with tick marks show crests of  
1965 tilted blocks on top of these detachments after Bécel et al. (2009). The detachment north  
1966 of the İmralı anticline is drawn on the basis of the SEISMARARA seismic profile in the  
1967 İmralı Basin, shown in fig 2b of Laigle et al. 2008. The location of this profile is shown by  
1968 the red line. See text. M1 is the Marmara 1 industrial well.

1969

1970 *Figure 3b*

1971 Enlargement of figure 3a.

1972

1973 *Figure 3c*

1974 Stacked profiles from East to West with erosional contours on top of it.

1975

1976 *Figure 4*

1977 Detail of contours of anticline around Marmara Island. Red line, SMF. Yellow barbed  
1978 lines, direction of propagation of clastics. The top of the Upper Miocene Kirazlı  
1979 formation rises abruptly across the normal fault to less than 250 m. near the island. The  
1980 log of the Marmara 1 drill hole situated to the east of Marmara Island is given for  
1981 reference. See Fig.3a and Le Pichon et al. (2014).

1982

1983 *Figure 5*

1984 Interpreted lithospheric SW-NE profile (see location on figure 7). Fault locations from Le  
1985 Pichon et al. (2014) and Laigle et al. (2008), supra-crustal model based on Bayrakci et al.  
1986 (2013), detachment geometry based on Bécél et al. (2010) and Moho depth from Kende  
1987 et al.( in prep.) model. TPAO line interpretations were also consulted to constrain the  
1988 fault and sediment deposition geometries on the Southern shelf. Violet faults represent  
1989 the Main Marmara Fault system in the Central Basin. Black dots are micro seismicity  
1990 localizations from Kandilli Observatory data. For comparison, we have shown at the  
1991 same scale below the profile the sketch of Jolivet et al. (2010) that illustrates the  
1992 possible future evolution of the Gulf of Corinth. Green, phyllite, quartzite. Grey, ductile  
1993 domain.

1994

1995 *Figure 6*

1996 Distribution of the marine Alçitepe Formation (uppermost Miocene–lower Pliocene, 5.3-  
1997 3.7 to 3.4 Ma) in blue and the Pliocene undifferentiated continental deposits in yellow  
1998 after the 1/500 000 map of the General Directorate of Mineral Research and Exploration  
1999 (2002), Görür et al. (1997) and Sakıncı et al. (1999). Map of decollements and anticlines  
2000 from figure 3a. Red pattern: deformation zone along the SMF.

2001

2002 *Figure 7*

2003 Moho topography in meters after Kende et al. (in preparation). See text. The thick black  
2004 line is the MMF. Blue line is location of figure 5 profile. Detachments contours and block  
2005 crests as in figure 3a.

2006

2007 *Figure 8*

2008 “Basement” topography after Bayrakci et al. (2013) superposed to Moho depth contours  
2009 of figure 7 in meters. Basement is defined as having a seismic velocity larger than 4.2  
2010 km/s and does not coincide everywhere with crystalline basement. Thick black line:  
2011 MMF. Yellow lines: contours of detachments as in figure 7. Submarine fault scarps after  
2012 Armijo et al. 2002 are represented in white. Black crosses are inverted nodes and red  
2013 ones are fixed nodes in the inversion of Bayrakci et al. (2013).

2014

2015 *Figure 9*

2016 Synthesis of information on age of onset of sedimentation in the newly formed North  
2017 Marmara Trough from Grall (2015, in preparation).

2018

2019 *Figure 10*

2020 Compilation of different data along a transect following the MMF. a) Map of the Sea of  
2021 Marmara. MMF in red based on Şengör et al. (2014) and contour lines of the Moho depth  
2022 from figure 7 b) Subsidence rate along the MMF retrieved from various studies (see  
2023 details in this paper). Dotted line indicates a lack of information to determine the  
2024 uncertainty. c) Fault plunge along the fault (see details in this paper). d), e) and f)  
2025 Crustal thickness, sediment thickness and Moho depth from Bayrakci et al. (2013)  
2026 basement model and Kende et al. (in prep) Moho model presented in figure 7.

2027

2028 *Figure 11*

2029 Topography of the Anatolia-Aegea area. Note the 2 000 meters altitude of the East  
2030 Anatolia Plateau, opposite the Arabian indenter and the progressive decrease of the  
2031 elevation westward to less than sea level below the Aegean Sea. The depth contours of  
2032 the Aegean slab are shown in dashed black lines. The fast-wave polarization axes of  
2033 shear waves detected by Paul et al. (2014) are also shown (red their measurements,  
2034 blue previous measurements). Note the progressive counterclockwise rotation of the  
2035 axes as one gets closer to the Aegean slab. The E/W profiles along 39.5°N show the  
2036 smoothed topography in blue and the crustal thickness in red after Karabulut et al.  
2037 (2015).

Draft

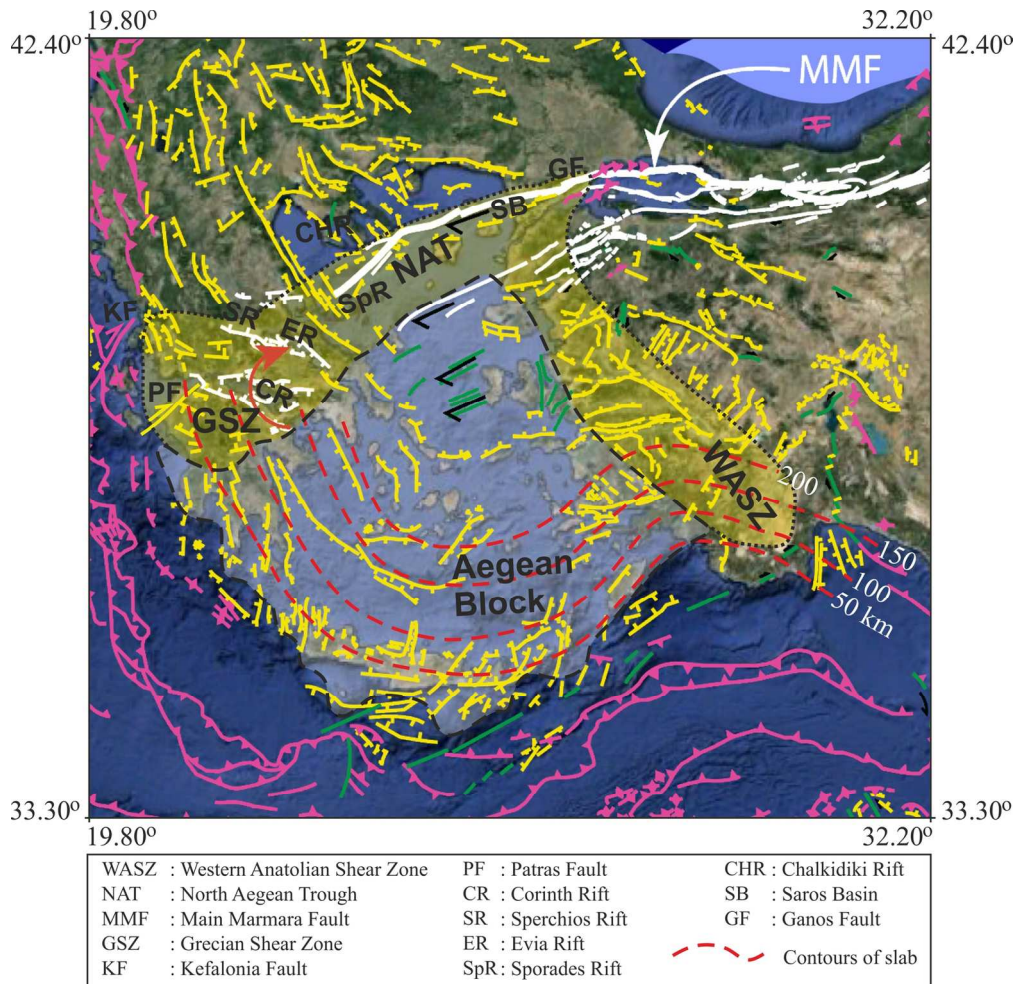
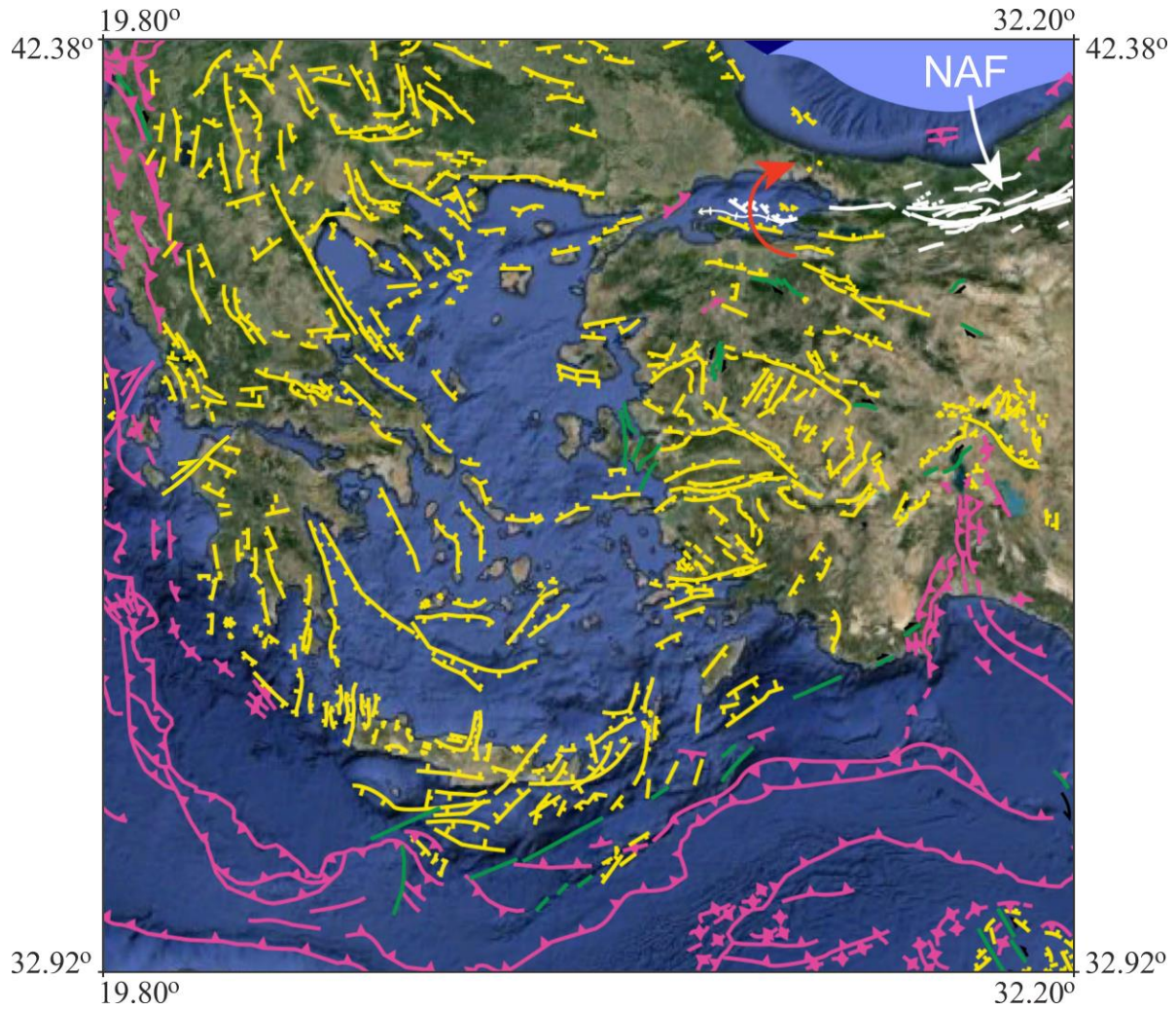
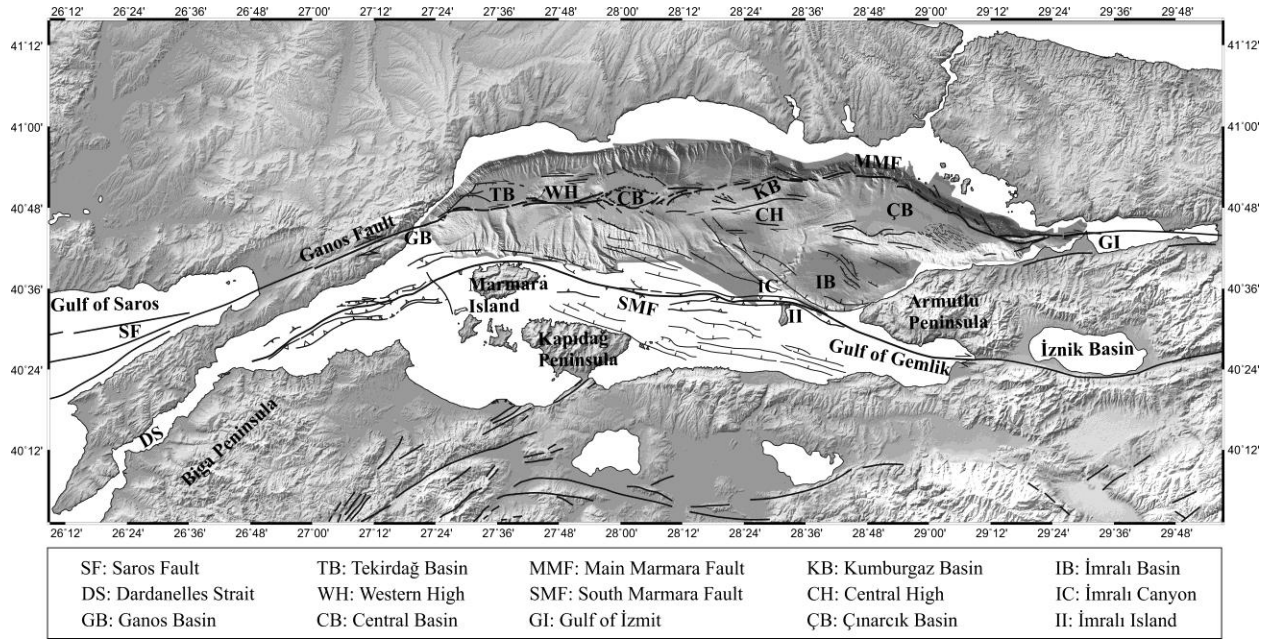


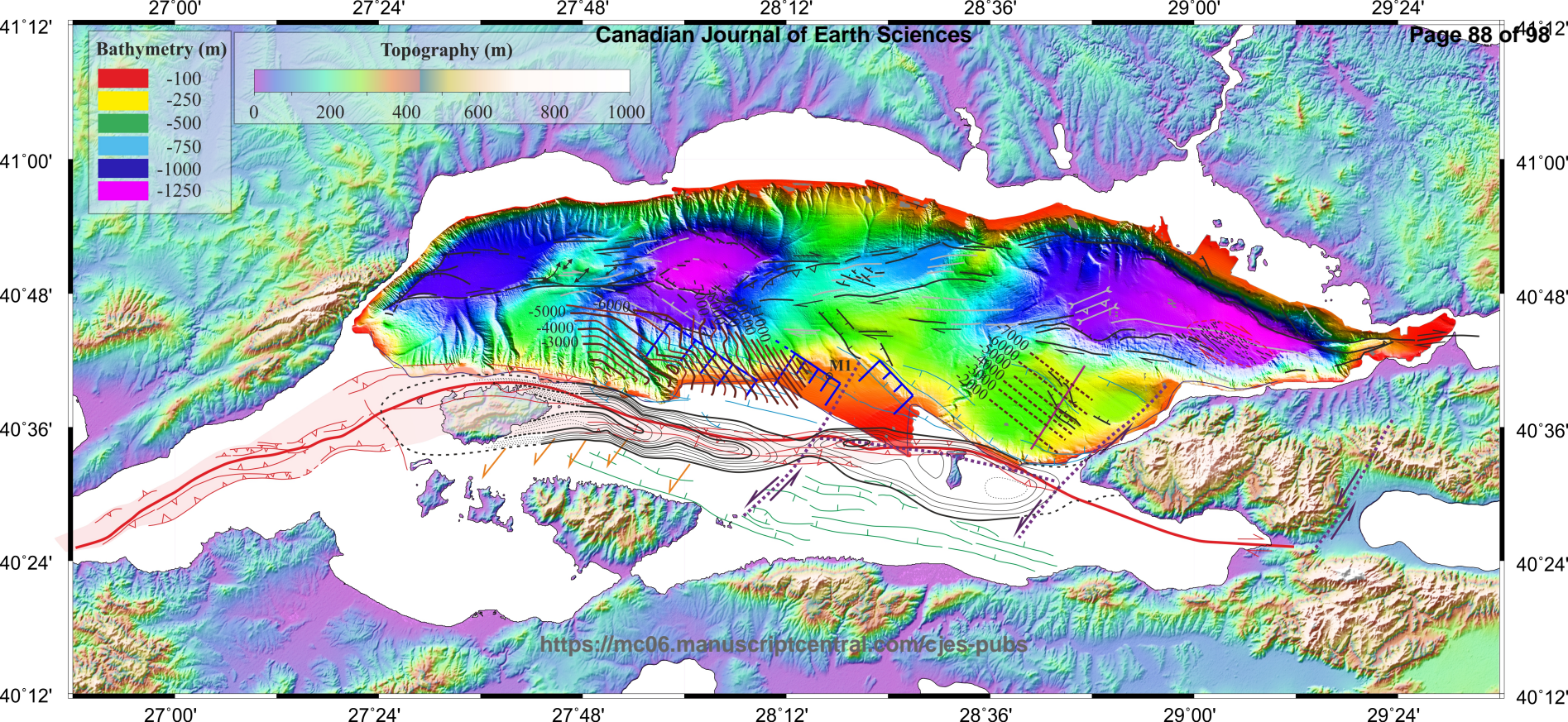
Figure 1  
153x149mm (300 x 300 DPI)

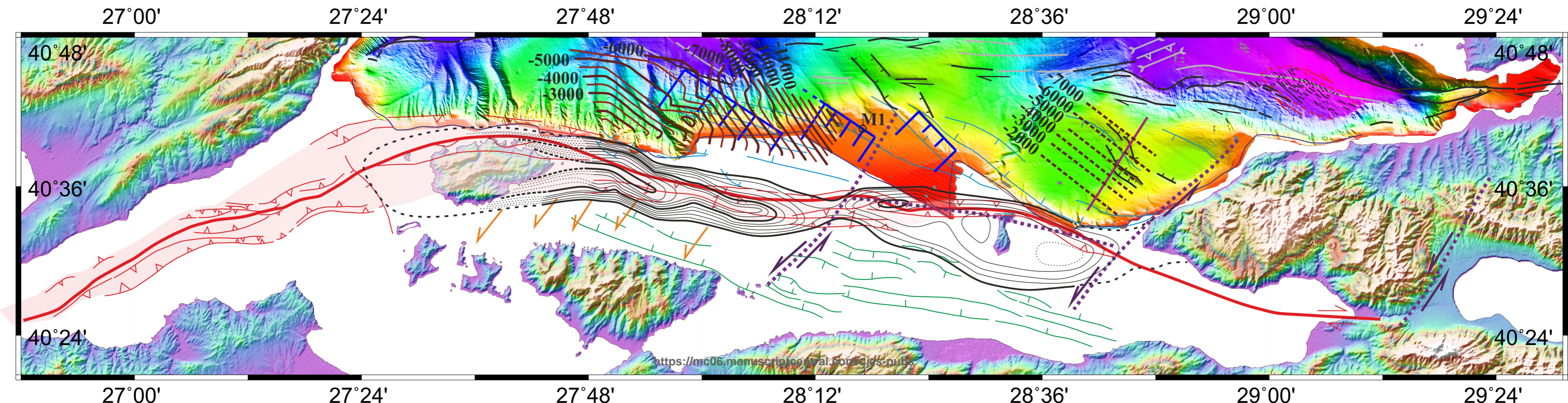
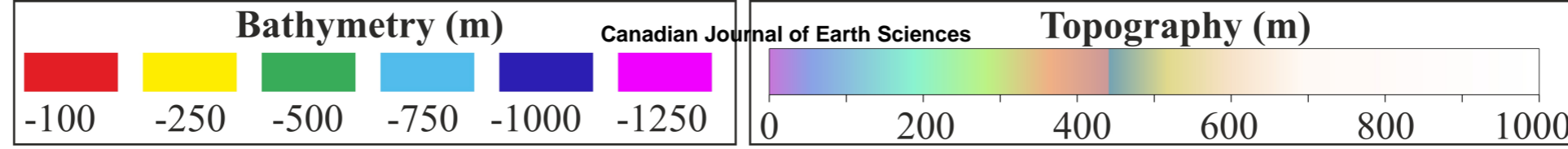






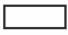

Draft

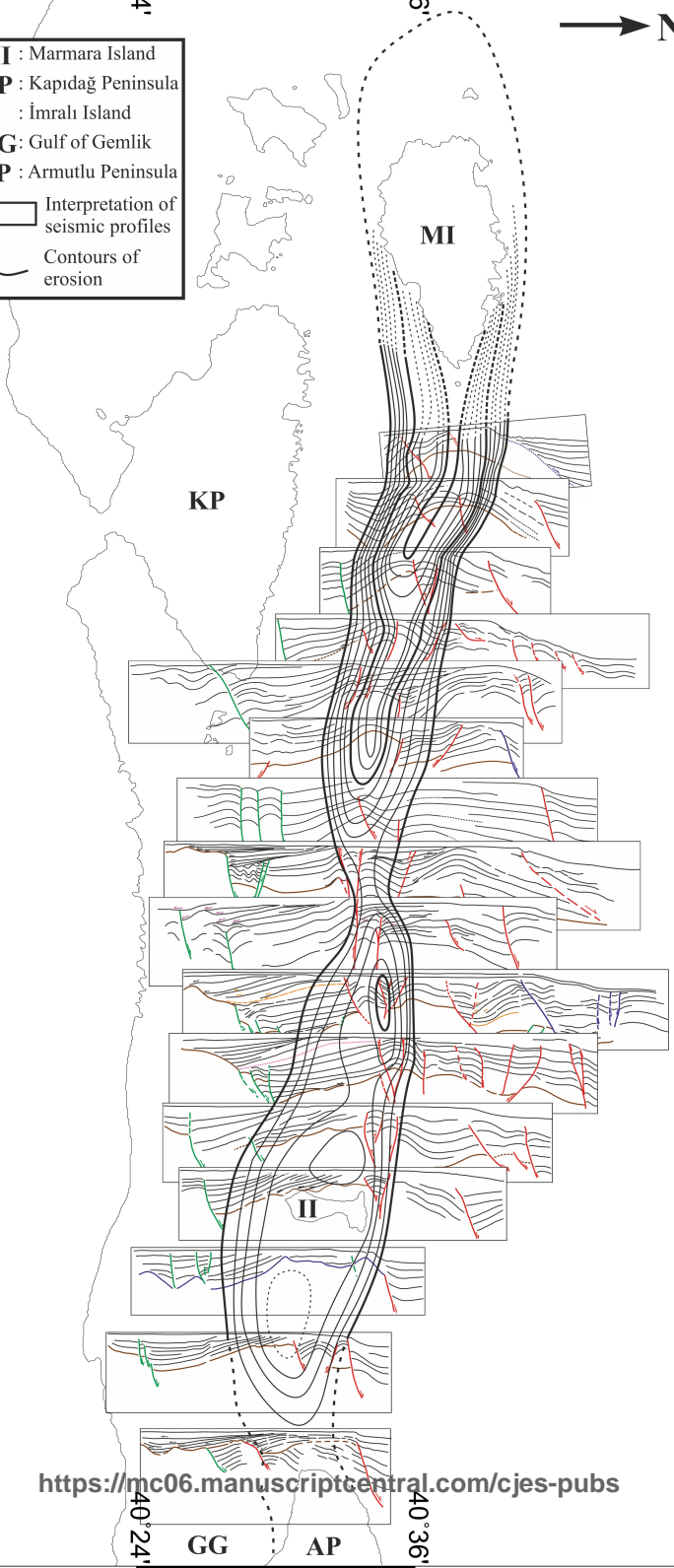




27°24'  
27°48'  
28°12'  
28°36'

27°24'  
27°48'  
28°12'  
28°36'

- MI** : Marmara Island
- KP** : Kapıdağ Peninsula
- II** : İmralı Island
- GG** : Gulf of Gemlik
- AP** : Armutlu Peninsula
-  Interpretation of seismic profiles
-  Contours of erosion



40°24' GG AP 40°36'

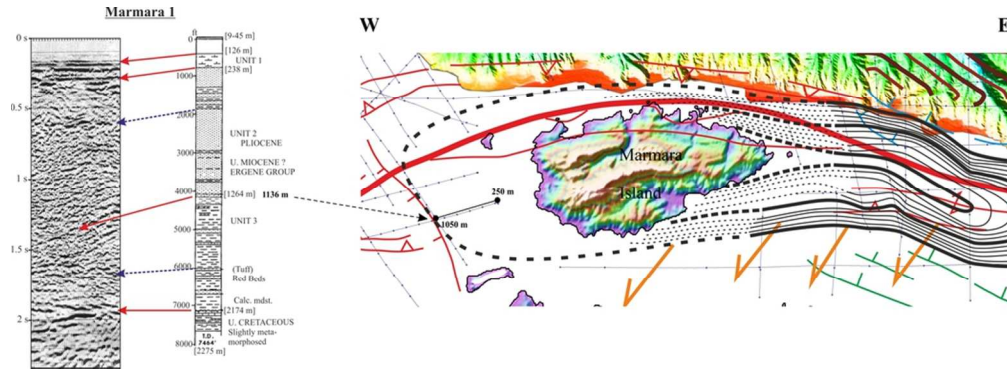


Figure 4  
88x32mm (300 x 300 DPI)

Draft

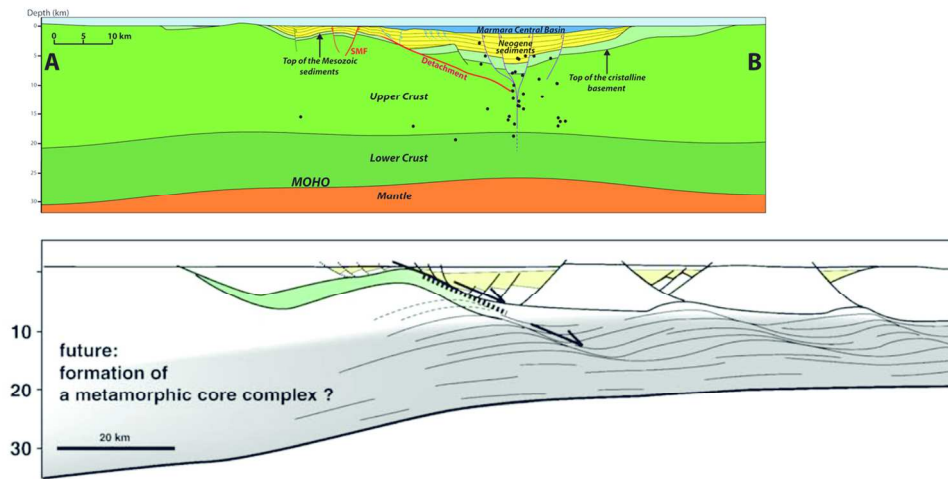


Figure 5  
126x62mm (300 x 300 DPI)

Draft

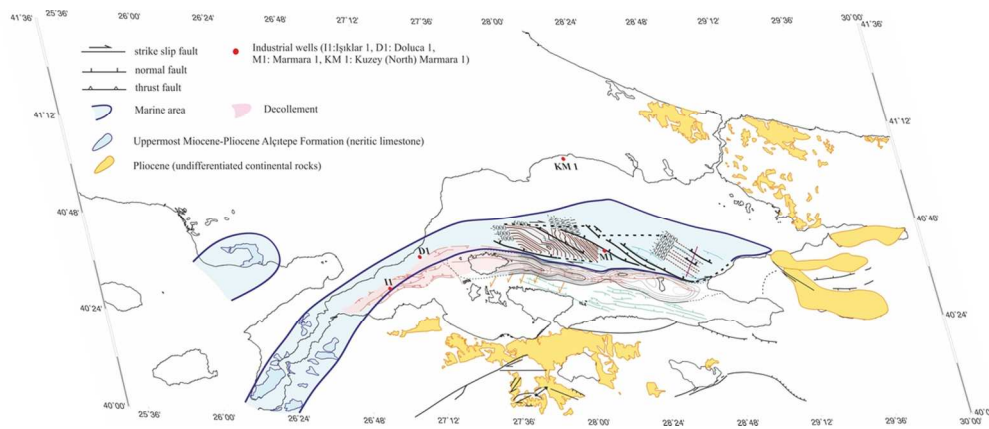


Figure 6  
106x44mm (300 x 300 DPI)

Draft

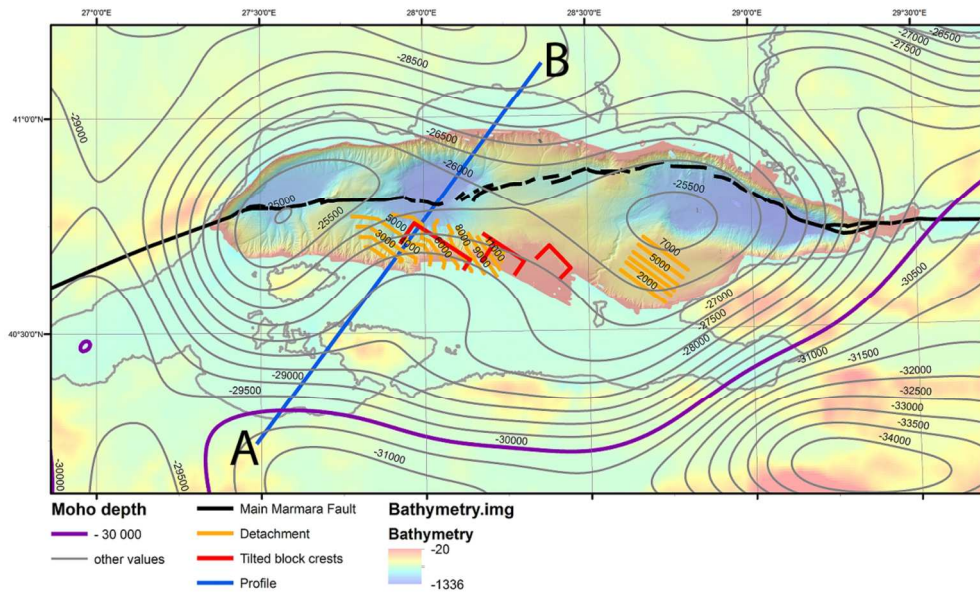


Figure 7  
160x96mm (300 x 300 DPI)



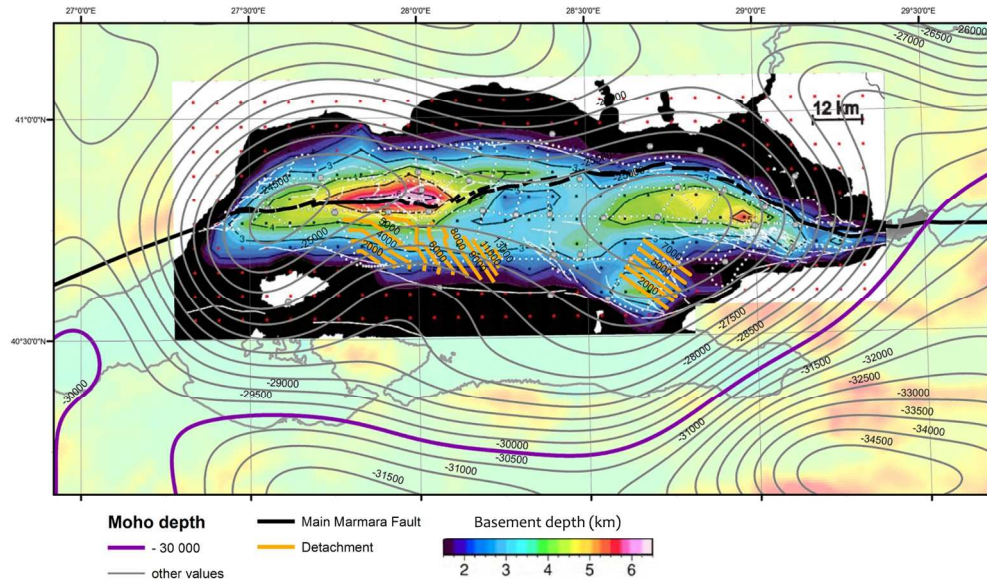


Figure 8  
157x93mm (300 x 300 DPI)

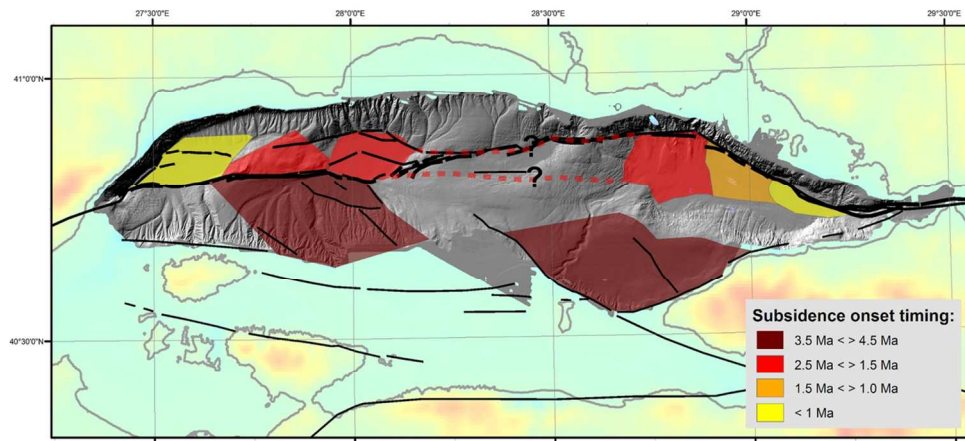


Figure 9  
126x58mm (300 x 300 DPI)

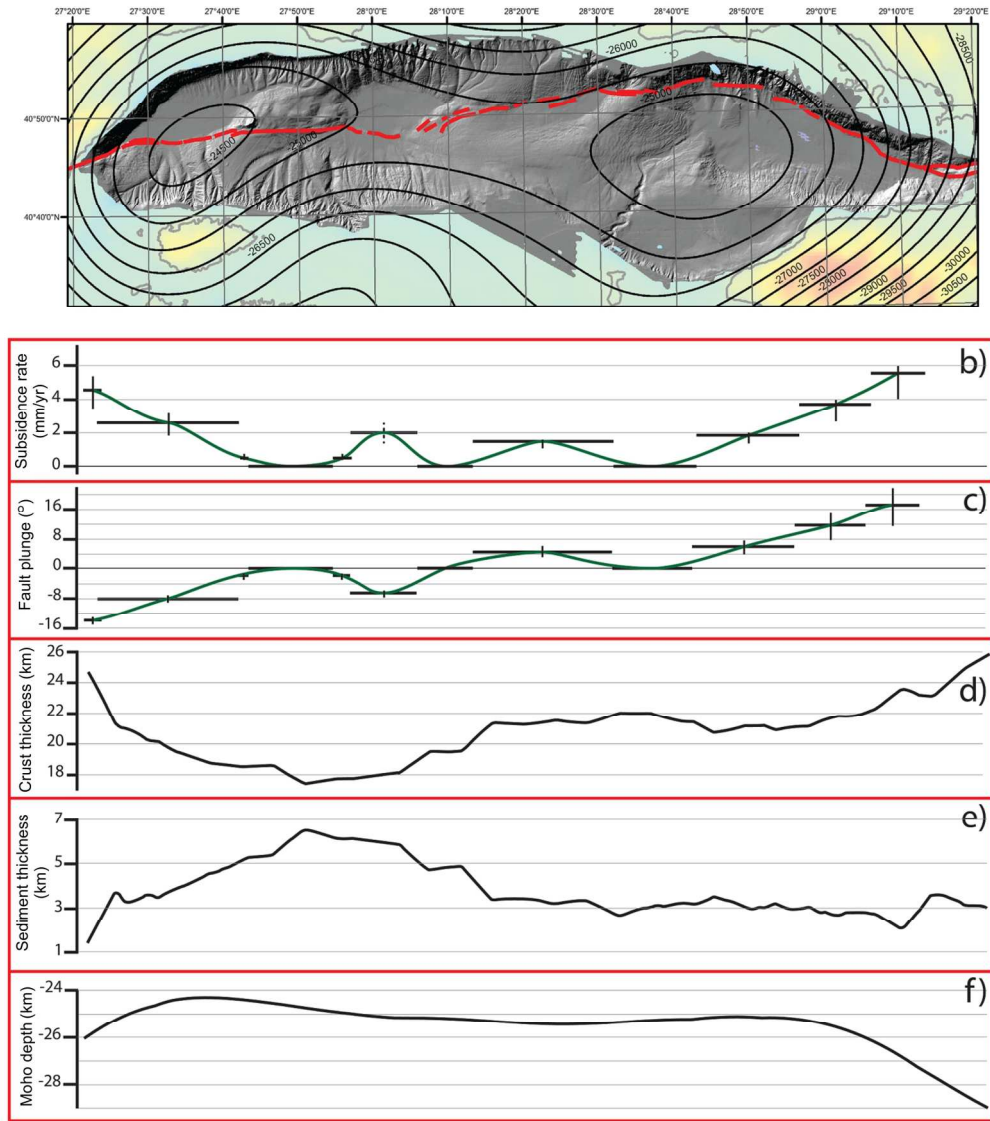


Figure 10  
174x195mm (300 x 300 DPI)

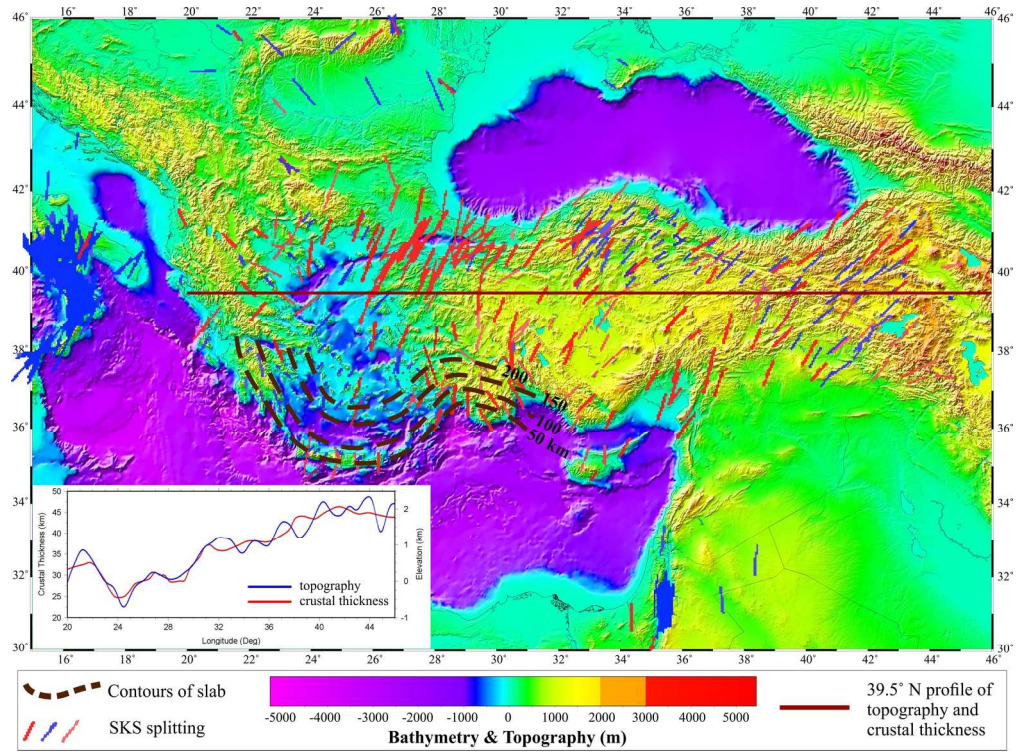


Figure 11  
176x130mm (300 x 300 DPI)